Aus dem

Hertie Institut für klinische Hirnforschung

Abteilung Zellbiologie Neurologischer Erkrankungen

RNF170 - a novel disease gene causing Hereditary Spastic Paraplegia

Inaugural-Dissertation
zur Erlangung des Doktorgrades
der Medizin

der Medizinischen Fakultät
der Eberhard Karls Universität
zu Tübingen

vorgelegt von

Gehweiler, Ina Sophie

2024

Dekan:	Professor Dr. B. Pichler
1. Berichterstatter:	Professorin Dr. R. Schüle-Freyer
2. Berichterstatter:	Professor Dr. S. Ossowski
Tag der Disputation:	13.11.2024

Für Beate Heßbrüggen
und Theresia Gehweiler

Table of Contents

List of Abbreviations

Abbreviation	Description
A	Adenine
AB	antibody
ACMG	American College of Medical Genetics and Genomics
ADSA	Autosomal dominant sensory ataxia
Ala	Alanin
ALS	Amyotrophic lateral sclerosis
ANOVA	Analysis of variance
APS	Ammonium persulfate
AR	autosomal recessive
Arg	Arginine
Asn	Asparagine
ATL1	Atlastin
BCA	Bicinchoninic acid
Bp	Base pairs
BSA	Bovine serum albumine
C	Cytosine
CADD score	Combined Annotation Dependent Depletion score
Cas9	CRISPR-associated protein 9
cDNA	Complementary Deoxyribonucleic acid
CNV	Copy number variation
CRISPR	Clustered Regularly Interspaced Short Palindromic Repeats
Cys	Cysteine
ddH_2O	Double distilled H_2O
DMEM	Dulbecco's Modified Eagle's Medium
DNA	Deoxyribonucleic acid
DNAH5	Dynein Axonemal Heavy Chain 5
dNTPs	Deoxyribonucleotide triphosphate
dsDNA	Double-stranded deoxyribonucleic acid
DTT	Dithiothreitol
E.coli	Escherichia coli
e.g.	*Exempli gratia*
ECL	enhanced chemiluminescence
EDTA	Ethylenediaminetetraacetic acid
ER	Endoplasmic reticulum
ERAD	Endoplasmic Reticulum-associated degradation
ERLIN 1/2	Endoplasmic reticulum lipid raft-associated protein 1/2
EtOH	Ethanol
EVS	Exome Variant Server
ExAC	Exome Aggregation Consortium
FBS	Fetal bovine serum
FCRL2	Fc Receptor Like 2

Fw	Forward
G	Guanine
GAPDH	Glyceraldehyde 3-phosphate dehydrogenase
gnomAD	Genome aggregation Database
GPR98	G-protein coupled receptor 98
GQ	Genotype quality filter
H_2O	water
het	heterozygous
hg19	human genome 19 (reference genome)
hom	homozygous
HRP	Horseradish peroxidase
HSP	Hereditary spastic paraplegia
HTT	Huntingtin
IP3	Inositol trisphosphate
IP3R1-3	Inositol trisphosphate receptor subtype 1-3
iPSCs	induced pluripotent stem cells
kDA	kilo Dalton
KO	knockout
LL	Lower limb
LOF	Loss of function
m	meters
MAF	minor allele frequency
MDa	Megadalton
moi	mode of inheritance
MOPS	3-(N-morpholino) propanesulfonic acid
MRC scale	Medical research council scale for muscle strength
MRI	magnetic resonance imaging
mRNA	Messenger RNA
n. d.	not done
NaAc	Sodium acetate
NGS	Next-generation sequencing
NMD	Nonsense mediated (RNA) decay
OMIM	Online Mendelian Inheritance in Man
PAGE	Polyacrylamide gel electrophoresis
PBS	Dulbecco’s phosphate buffered saline
PCR	Polymerase chain reaction
PLS	Primary lateral sclerosis
PolyPhen	Polymorphism Phenotyping (Prediction tool)
PVDF	Polyvinyl difluoride
qRT-PCR	Quantitative real time polymerase chain reaction
QUAL	Quality filter (GENESIS specific filter)
REEP1	Receptor expression-enhancing Protein 1
RIPA	Radioimmunoprecipitation assay (lysis buffer)
RNA	Ribonucleic acid
RNF170	Ring Finger Protein 170

RT	Room temperature
RT	Room temperature
RT-PCR	Real time polymerase chain reaction
RTN2	Reticulon 2
Rv	Reverse
RyR	ryanodine receptor
SCA	Spinocerebellar ataxia
SDS	Sodium dodecylsulfate
SH-SY5Y	Human neuroblastoma cell line SH-SY5Y
SPAST	Spastin
SPG	Spastic paraplegia gene
SPRS	Spastic Paraplegia Rating Scale
T	Thymine
TBS	Tris buffered saline
TBS-T	Tris buffered saline + 0,1% Tween 20
TEMED	Tetramethylethylenediamine
UCSC	University of California, Santa Cruz
UL	Upper limb
UPP	Ubiquitin - proteasome pathway
VE water	Demineralized water
WES	Whole exome sequencing
WGS	Whole genome sequencing
y	years
ZNF646	Zink Finger Protein 646

List of Tables

List of Figures

1. Introduction

1.1 Hereditary Spastic Paraplegias

Hereditary spastic paraplegias (HSP) are a clinically and genetically extremely heterogeneous group of monogenic neurodegenerative disorders. With a prevalence of 2-10/100.000 they are counted among the rare diseases (Braschinsky *et al.*, 2009; Erichsen *et al.*, 2009; Klebe, Stevanin and Depienne, 2015). Their most prominent feature is a length dependent axonopathy of the corticospinal tract motor neurons leading to the cardinal symptoms of progressive lower limb spasticity and weakness. To date mutations in more than 80 genes are known to cause HSP (Novarino *et al.*, 2014).

To understand the pathology of HSPs a short neuroanatomical digression is required. The human voluntary motoric nervous system which is necessary for any controlled skeletal muscle movements is composed of two main neuronal tracts. It starts with the upper motor neurons, which descend predominantly from layer V of the motor cortex and form the corticospinal tract. These corticospinal tract axons predominantly decussate in the caudal medulla and follow the lateral tract or partially follow the anterior tract until decussation on spinal cord level. After decussating these axons synapse either directly in the anterior horn of the spinal cord onto lower motor neurons or via spinal interneurons. These lower motor neurons form the second level and transmit their action potentials via neuromuscular synapsis to their respective muscle.

As the corticospinal tract motor neurons can reach a length of up to one meter, they form the longest axons of the human body. This enormous length enables them on the one hand to perform extremely fast nerve conduction. On the other hand, due to the great complexity of the required axonal transport mechanisms it creates a high vulnerability of this cells, which makes them susceptible to distal axon degeneration resulting in neurodegenerative diseases such as HSP.

The clinical hallmark of all forms of HSP is a progressive spastic gait disorder resulting from the axonopathy of the upper motor neurons. According to the

clinical findings HSPs can be classified into two broader subgroups (Harding, 1983). The ‘pure’ form describes an isolated pyramidal syndrome with predominantly lower limb spasticity sometimes accompanied by neurogenic bladder disturbances or impaired vibration sense. The ‘complicated’ forms are characterized by the affection of additional neurological and non-neurological systems and therefore variably include additional symptoms such as optic atrophy, retinitis pigmentosa, cognitive impairment, dementia, cerebellar ataxia, seizures and peripheral neuropathy (Fink, 2013).

HSPs are highly variable both in age of onset, ranging from early childhood to late adulthood and disease severity with mild and barely disabling lower limb spasticity up to inability of walking and permanent use of a wheelchair (Ruano *et al.*, 2014; Klebe, Stevanin and Depienne, 2015). Also progression of disease manifestation can vary from generally slow progression over decades to rapid decline of lower limb voluntary movements usually without a shortened life expectancy (Schüle and Schöls, 2011; Klebe, Stevanin and Depienne, 2015). Progression velocity, age of onset and disease severity partially correlate with the underlying genetic defect, but still have a high variability even upon members of the same family (Fink, 2013; Klebe, Stevanin and Depienne, 2015; Schüle *et al.*, 2016). The Spastic Paraplegia Rating Scale (SPRS) (Schüle *et al.*, 2006) is widely used to monitor disease progression in HSP. Due to the high variability of HSPs it remains challenging to give patients a clear clinical prognosis or prediction of the expected disease manifestations as it comes to genetic counseling.

To date, there are no causal therapeutic strategies for the treatment of HSP. Symptomatic therapies, such as antispastic drugs to reduce muscle spasticity and pain, or medical treatment of the neurogenic bladder disturbances are commonly used treatment strategies. In addition, patients benefit greatly from regularly performed physiotherapy to improve or at least preserve gait pattern and mobility.

Regarding the genetics HSPs are among the most heterogeneous Mendelian disorders. Modes of inheritance include autosomal dominant, autosomal

recessive and x-linked inheritance patterns (Schüle and Schöls, 2011). For a long time HSP has been a diagnosis of exclusion, but since emerging genetic testing came up, a variability of genes causing HSP have bene discovered over the last few decades.

After the first HSP locus was identified in 1986 (Kenwrick *et al.*, 1986), nowadays almost 80 HSP loci have been identified and termed numerically as spastic paraplegia genes (SPG) according to their order of discovery (Figure 1) (Schüle and Schöls, 2011; Lo Giudice *et al.*, 2014). In fact, the so called SPGs only represent a subset of more than 100 genes known to cause HSP which already has been cataloged by OMIM (www.omim.org). Yet, about one third of cases still remains unexplained by mutations in known genes (Schüle *et al.*, 2016). Therefore, further genetic heterogeneity seems likely.

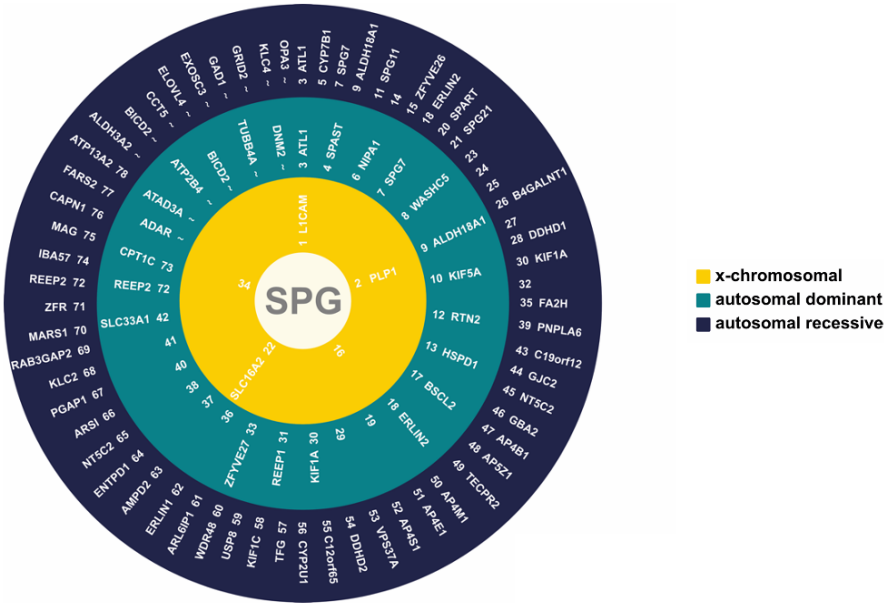

Figure 1: Schematic illustration of the ~ 80 known spastic paraplegia genes (SPG) with their mode of inheritance. *Genes are sorted by their mode of inheritance and labeled numerically according to their order of discovery as SPG 1-72. For some of the HSP loci established by linkage, the causative gene has not been identified yet (adapted from © Schüle R., Springer Verlag, updated after (Hedera, 2021)).*

1.1.1 Common pathophysiological mechanisms in HSP

With the progressive discovery of numerous causative genes for HSPs, the understanding of the underlying cellular mechanisms responsible for motor neuron axonopathy has greatly improved.

In order to organize these disease genes and the resulting proteins into functional groups several classifications have been proposed. Blackstone (Blackstone, 2012) for example, proposed a division into four functional groups (membrane trafficking, mitochondrial regulation, myelination and lipid modification, axon pathfinding) whereas Klebe (Klebe, Stevanin and Depienne, 2015) allocated the gene products to five functional groups (axonal transport, intracellular trafficking, mitochondrial function, lipid metabolism, development and myelination).

Moreover, many of the altered proteins play a role in more than one of these groups or interact in a larger connective network (Klebe, Stevanin and Depienne, 2015).

Figure 2 demonstrates the assignment of the most common SPGs to these functional groups as well as their cellular localization in a neuronal cell. It demonstrates how many pathophysiological mechanisms are involved in HSP overall and points out that most HSP gene products are involved in the group of 'intracellular trafficking'. Among these, numerous of the altered proteins, such as spastin (SPAST), atlastin (ATL1), Receptor expression-enhancing Protein 1 (REEP1), erlin2 and reticulon2 (RTN2) interact in shaping the tubular endoplasmic reticulum (ER) morphology, implying that this may be one of the most common pathophysiological mechanisms in HSP.

However, the ER has many different functions and it remains unclear which ones have the most pathogenetic relevance (Blackstone, 2012).

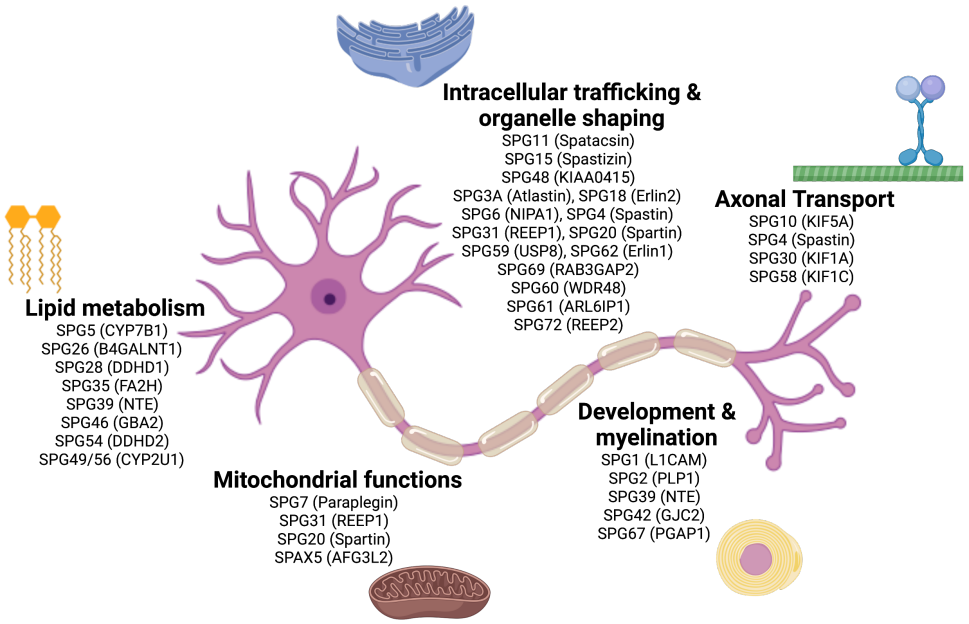

Figure 2: Schematic of a neuron giving an overview of the main pathophysiological mechanisms in HSP. *The most common SPGs (and respective genes) are organized in five functional groups according to their cellular function and localization (adapted from Klebe, Stevanin and Depienne, 2015, created with BioRender.com).*

1.2 The use of GENESIS for WES/WGS data analysis

The widespread use of next-generation sequencing (NGS) technologies in the recent years has revolutionized genetic research (van Dijk *et al.*, 2014). NGS offers the possibility of low-cost, rapid, high-throughput, parallel sequencing, which has already led to the identification of numerous disease genes for Mendelian disorders (Ng *et al.*, 2010; Velinov *et al.*, 2012). The rapid increase in new gene discoveries results on the one hand from the enormous amount of affordable Whole exome sequencing (WES) and Whole Genome sequencing (WGS) data, on the other hand from the development of effective filtering strategies to identify a small number of potential candidate genes as causative variants in the respective patient (Gonzalez *et al.*, 2015).

Therefore, several tools have already been developed to process and visualize this huge amount of genetic data inter alia GENESIS. The GENESIS platform was used in this work to identify novel disease genes for HSP because it

provides a user-friendly and highly customized analysis of NGS data even for users without bioinformatical background (Gonzalez *et al.*, 2013).

Many gene discoveries have led to deeper understanding of the underlying cellular mechanisms responsible for disease development especially in Mendelian disorders. Therefore, identifying new disease genes is a crucial step in order to investigate disease causing pathophysiological mechanisms and develop possible future targeted therapies (Biesecker, 2010; Gonzalez *et al.*, 2015).

In this work we performed a step wise analysis approach on NGS data of two siblings using the automated pipeline of GENESIS and identified a novel disease gene for HSP through subsequent genetic matchmaking with three additional families. The gene we found responsible to cause HSP, when biallelic mutated, is called *RNF170* and plays inter alia a crucial role in intracellular Ca^{2+} metabolism, which is why a detailed introduction to this particular metabolism is given in the following sections. To investigate possible intracellular functional effects of this newly discovered disease gene we used patient cells.

1.3 The use of fibroblasts as *in vitro* cell model

A common problem in the in vitro investigation of neurological diseases is to find an appropriate cell model. Since neuronal cells cannot be harvested from living patients for ethical reasons and patient-derived induced pluripotent stem cells (iPSCs) that can be differentiated into cortical neurons (Hauser *et al.*, 2016) are very expensive, human fibroblasts are a good alternative for many applications.

Human fibroblasts can be generated from living patients via skin biopsy, are easy to handle, low cost and well-tried, which is why they are often used as a cell model for primary patient-associated cell culture experiments.

For further investigation, SH-SY5Y cells are suitable for overexpression experiments, as these commercially available neuroblastoma cells (Kovalevich and Langford, 2013) are an easy and commonly used way to create an *in vitro* model for neurological diseases.

1.4 Inositol trisphosphate receptors and Ca^{2+} metabolism

Calcium metabolism plays an essential role for many regulatory processes in mammalian cells most notably in excitable cells, such as neurons (Pchitskaya, Popugaeva and Bezprozvanny, 2018). Especially the ER related Ca^{2+} release takes part in several cell signaling processes e.g. apoptosis, synaptic plasticity and autophagy (Foskett *et al.*, 2007).

Within the cell, the endoplasmic reticulum serves as a calcium store. Since the calcium concentration inside the ER is higher than in the cytoplasm, the resulting electrophysiological gradient can be used for cell signaling processes. Two types of calcium channels can be distinguished in the ER membrane, the inositol trisphosphate receptors (IP3R) and the ryanodine receptors (RyR) (Foskett *et al.*, 2007; Wagner *et al.*, 2019).

IP3Rs are large ER membrane proteins and form tetrameric complexes in the ER membrane thus building channels, which are activated by binding of inositol trisphosphate (IP3), leading to channel opening and efflux of calcium into the cytosol. The cytoplasmatic formation of IP3 is stimulated by various G-protein-coupled surface receptors in the plasma membrane. In mammalian cells there are three different subtypes of IP3R's (IP3R1, IP3R2, IP3R3), which differ slightly in terms of biochemical characteristics and distinctly in terms of their tissue-specific distribution (Foskett *et al.*, 2007). While subtype 3 (IP3R3) is predominant for example in fibroblasts, neuronal cells mainly express IP3R1, which is the subtype most widely expressed (Wojcikiewicz *et al.*, 2009).

Degradation of IP3Rs can be divided in stimulus-dependent receptor degradation and basal turnover. Within degradation after activation the newly synthesized channels are degraded directly after activation via the endoplasmic reticulum -associated degradation (ERAD) pathway, which marks the first step of the ubiquitin - proteasome pathway (UPP) for aberrant ER proteins (Khan and Joseph, 2003). After recognition of the activated channels they are most likely dislocated across the ER membrane (Olzmann, Kopito and Christianson, 2013) followed by polyubiquitination which leads to degradation by the proteasome and thus result in the UPP.

Only little is known to date about the basal turnover of IP3Rs. Apparently it takes longer than stimulus-dependent receptor degradation upon activation and there are studies postulating the involvement of lysosomal degradation as well as degradation via the UPP similar in IP3R turnover upon activation (Bokkala and Joseph, 1997; Khan and Joseph, 2003).

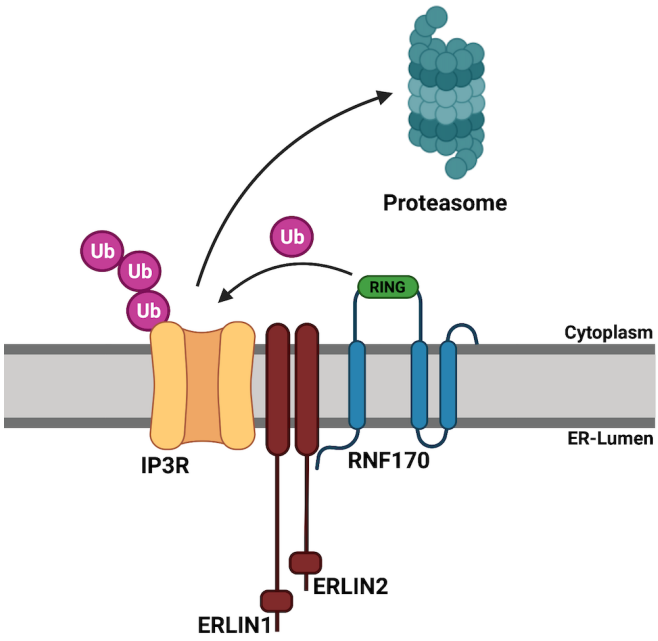

Figure 3: Simplified model of IP3R degradation via ERAD pathway. *Immediately after activation the IP3R is recognized by the ERLIN1/2 complex which recruits RNF170 to the opened channel. RNF170 mediates the ubiquitination of IPR3 followed by consecutive degradation via the UPP. ERAD: Endoplasmic Reticulum-associated degradation, Ub: Ubiquitin, RING: Ring-domain, IP3R: Inositol trisphosphate receptor, ERLIN1/2: Endoplasmic reticulum lipid raft-associated protein 1/2, RNF170: Ring Finger Protein 170, ER: Endoplasmic Reticulum, UPP: Ubiquitin - proteasome pathway (Created with BioRender.com).*

1.5 ERAD, ERLIN1/2 and RNF170

Nearly one third of all proteins of mammalian cells are synthesized in association with the endoplasmic reticulum. This huge amount of several proteins results in a multitude of different folded and oligomeric protein complexes, which is why degradation of these proteins is also a complex process mediated by the various players of the ERAD. Depending on the

respective protein, there are a wide variety of mediators and degrading proteins involved such as ligases, responsible for ubiquitination (Olzmann, Kopito and Christianson, 2013).

Activation-dependent IP3R degradation is mediated by the proteins endoplasmic reticulum lipid raft associated protein 1 and 2 (ERLIN1, ERLIN2) and the E3 ligase Ring Finger Protein 170 (RNF170). Thereby, the proteins ERLIN1 and ERLIN2 form a complex that recruits the RNF170 E3 ligase, which then ubiquitinates the activated receptors, thus delivering them to the UPP (Lu *et al.*, 2011) as shown in Figure 3.

The proteins ERLIN1 and ERLIN2 are each ~ 40 kDa in size and have a very similar structure. The major part of the single protein lies intraluminal and contains one transmembrane domain. Within the ER membrane, the two proteins form a complex of approximately 40-50 ERLIN1 and ERLIN2 subunits whilst connecting through their intraluminal assembly domains. This creates an oligomeric complex approximately 2 MDa in size, which mediates the before-mentioned interaction between the IP3Rs and RNF170 (Shenoy, 2016, p. 148). It is already known that different mutations in these two genes can cause HSP. More precisely mutations in *ERLIN1* have been associated with autosomal recessive SPG62 and in *ERLIN2* with autosomal recessive SPG18 (Alazami *et al.*, 2011; Novarino *et al.*, 2014).

RNF170 is a RING domain-containing protein that resides in the ER membrane and acts as a ubiquitin ligase to mediate the degradation of activated IP3Rs (Lu *et al.*, 2011). It is composed of three transmembrane domains and the cytosolic RING domain which is responsible for the ligase function (Shenoy, 2016, pp. 148 - 149). A founder mutation in RNF170 has been identified as disease causing variant in two Canadian families suffering from another neurodegenerative disease named autosomal dominant sensory ataxia (ADSA), which is phenotypically different from HSP (Valdmanis *et al.*, 2011).

1.6 Alterations in Ca^{2+} signaling as common pathophysiological pathway for neurodegenerative diseases

In addition to the aforementioned involvement in the pathogenesis of various HSPs, alterations in calcium metabolism as well play a role in other neurodegenerative diseases (e.g. spinocerebellar ataxias, Huntington´s disease, Alzheimer´s disease), which supports the increasing pathophysiological relevance of this pathway when it comes to neurodegeneration.

For example, it has been shown that impaired intracellular calcium metabolism underlies several forms of spinocerebellar ataxias (Chen *et al.*, 2008; Liu *et al.*, 2009; Kasumu *et al.*, 2012). These respective ataxias share this aspect of disease pathophysiology with Huntington´s disease, where the disease is caused by polyglutamine expansion of the underlying Huntingtin (*HTT*) gene. The resulting mutant protein in Huntington´s disease sensitizes inositol trisphosphate receptor subtype 1 to activation by IP3 thus leading to increased calcium release from the ER (Tang *et al.*, 2003).

Last but not least, evidence is accumulating that disruption of calcium homeostasis may play an early and major role in Alzheimer´s disease (Tong *et al.*, 2018).

Due to this multitude of neurodegenerative diseases in which calcium signaling plays an important role, this pathway more and more evolves as an interesting target for future therapeutic developments.

1.7 Objective of the thesis

HSPs are among the most heterogeneous Mendelian disorders. Although there are several mutations in many individual genes known to cause different forms of HSP, about one third of all families with HSP are unexplained by mutations in known disease genes. Moreover, monogenetic diseases like HSP have ´modeling character´ for other neurodegenerative diseases and the identification of the remaining HSP genes would greatly improve our

understanding of the pathogenic models in HSP and the functional networks leading to axon degeneration.

The aim of this study was the identification of novel genes causing HSP in order to find a genetic diagnosis for at least a few of this affected families and gain more information about the functional pathways underlying the disease. Therefore we applied a step-wise analysis approach to existing WES/WGS datasets of unsolved families to identify candidate genes. These candidate genes were used to perform genetic matchmaking to identify novel disease genes. Fortunately, whilst applying this analysis approach to our HSP cohort, we were able to identify a novel candidate gene in a family with two affected siblings rather quickly, which is why the focus of the following experiments shifted towards substantiating the causal link between the newly discovered candidate gene and the phenotype. All results were evaluated via Sanger sequencing and for further investigation of the newly discovered gene, additional functional experiments were conducted using fibroblasts and protein biochemical methods.

The results present the newly discovered HSP gene *RNF170* and give an insight into the role of inositol 1,4,5-trisphosphate signaling as an upcoming key pathway for HSPs which allows speculations about possible future pathway oriented therapies.

2. Material and Methods

2.1 Sample Collection

The study was approved by the local institutional review board (Ethikkommission) at the University of Tübingen (054/2013BO1). Data was collected at the department of neurology of the University Hospital Tübingen. All patients and healthy control subjects gave their written and informed consent to the study including clinical data collection, collection and storage of biological samples and further experimental analyses.

2.2 In silico analysis of WGS data via GENESIS

2.2.1 Screening for variants in known disease associated genes

Among a cohort of 142 individuals with genetically unsolved HSP for which WES and WGS datasets were available, we focused on a family with presumably autosomal recessive mode of inheritance (HIH 19851). In this family, WGS datasets of the two affected siblings (H.4, H.5) were available. WGS data was generated using TruSeq PCR-free sample preparation (Illumina, San Diego, USA) and sequencing on a HiSeq X HD v2.5 instrument (Illumina, San Diego, USA). Processing of WGS data and analysis was performed using the GENESIS pipeline (Gonzalez *et al.*, 2015). 99,77% of the more than 1.684.998.067 reads with an average length of 150bp and average read depth of 34,75 could be mapped to the UCSC human reference assembly (hg19).

In the first analysis step we performed a screening for mutations in known HSP genes by in silico analysis. Hereby we used a hand-curated gene list containing 289 genes known to cause HSP and 279 additional genes associated to other neurodegenerative diseases of multisystemic phenotype including spasticity as well as other symptoms common to complicated HSP. The complete gene list used for screening is shown in the supplement (Table 20).

2.2.2 Genetic filtering for candidate gene identification

As the screening for rare coding variants in the known HSP genes revealed no molecular diagnosis we went on to the next analysis step. According to the family tree we assumed an autosomal recessive mode of inheritance and therefore we filtered the WGS data from the two affected siblings (H.4, H.5) for homozygous or compound heterozygous variants. To further narrow down the remaining variants and strengthen their validity as strong candidate genes we applied certain quality filters (Read depth > 8, Genotype quality filter (GQ) > 50 or Quality filter (QUAL) > 35) and chose a minor allele frequency (MAF) < 1% in ExAC, EVS and 1000 Genomes and an allele count < 21 in 5900 individuals in the GENESIS database. Afterwards the resulting candidates underwent sanger sequencing based segregation analysis.

2.2.3 Genetic matchmaking via gene matcher

To supply additional genetic proof for the pathogenic relevance of the remaining candidate gene (*RNF170*), the gene was posted at the GeneMatcher platform (Sobreira *et al.*, 2015) which allows researchers to post a gene of interest and links them directly to others who posted the same gene.

2.3 Sequencing analysis of candidate variants

2.3.1 Amplification Polymerase Chain Reaction

To validate the candidate variants from the in-silico analysis of WES/WGS data Sanger sequencing was performed. Therefore, in a first step a Polymerase Chain Reaction (PCR) was used to amplify the region of interest with specific primers designed to bind to regions flanking the relevant mutation. All primers were purchased from Integrated DNA Technologies (IDT, Coralville, IA/USA) and are shown in Table 1.

Table 1: Specific primer pairs for candidate gene validation

Name	Position (hg19)	Primer sequences (5'-3')
DNAH5	chr5:13714683T>C chr5:13714547+13714737	Fw: CAGCATATCATCAGCCAGCC Rv: TTGTTCAGAGTTTGCCTGCC
DNAH5	chr5:13716802G>A chr5:13716768+13716990	Fw: ATCATGTAGCGGATGGTGGT Rv: TCATGGACCTGAGCACTGAG
FCRL2	chr1:157737105C>T chr1:157737006+157737299	Fw: GTAACACCCACCCACCTGAG Rv: TTCCAGTGTCTCGCCCTG
FCRL2	chr1:157738309G>T chr1:157738218+157738369	Fw: TTCACCACCTTGCTCTGGAT Rv: TACAGAGAGGCCACAGGAAC
GPR98	chr5:89925235G>T chr5:89925107+89925340	Fw: CAGCCCAGGTGAACGATACT Rv: GCTCCATTTTGAAGGAATGC
GPR98	chr5:90012539G>A chr5:90012420+90012636	Fw: TGCACAAGGATTGTTTGGAA Rv: CATTCTAGGACTTGAGTGCTCATC
RNF170	chr8:42720556T>C chr8:42720341+42720777	Fw: AGGAAGCTACGATCATGCCA Rv: AAGGGTTGGCTGGATGAAGT
ZNF646	chr16:31090120C>G chr16:31090048+31090292	Fw: ACCCAACTCCTCTTCCCACT Rv: AGAGGAAAGGCTGTGCTGAG
ZNF646	chr16:31090182G>T chr16:31090048+31090292	Fw: ACCCAACTCCTCTTCCCACT Rv: AGAGGAAAGGCTGTGCTGAG

* DNAH5: Dynein Axonemal Heavy Chain 5, FCRL2: Fc Receptor Like 2, GPR98: G-protein coupled receptor 98, RNF170: Ring Finger Protein 170, ZNF 646: Zink Finger Protein 646

After diluting DNA and primers to the required concentrations all reagents were placed on ice. To pipette the master mix ddH_2O, 5 x Green GoTaq Reaction Buffer (Promega, Madison, USA), 10 mM dNTPs (Thermo Fisher Scientific, Waltham, USA), primers and the G2 GoTaq polymerase (Promega, Madison, USA) were mixed in PCR tubes as shown in Table 2.

Table 2: Master mix for amplification PCR reaction

Components	**Volume [µl]**
Green Go Taq Reaction Buffer (5x)	5
dNTPs (10 mM)	0,5
Primer fw+rv (10µM)	1,25
Go Tag polymerase (Promega 5 U/µl)	0,25
DNA-sample (10 ng/µl)	2,5
dd H_2O	15,5
Total	**25**

For amplifying the region of interest both forward and reverse primers were used in the same reaction. Finally, the DNA was added to the approach and the tubes were put into the T100^{TM} Thermal Cycler (Bio-Rad Laboratories, Hercules, CA/USA), applying the protocol shown in Table 3.

Table 3: PCR program for general amplification

Step	**Temperature (°C)**	**Time**	**Cycles**
Preheating	94 °C	5 min	
Denaturation	94 °C	30 sec	35 x
Annealing	62 °C	30sec (T_A)	
Elongation	72 °C	30sec	
Final elongation	72 °C	10min	
Cooling	4 °C	forever	

Afterwards, 5µl of the PCR product were used for Agarose gel electrophoresis to check whether the desired product was amplified, whilst the remaining 20µl were purified for subsequent sequencing PCR.

For purification 40µl sodium acetate/ethanol (NaAc/EtOH with 3 M NaAc pH 5.2 1:25 in 100 % EtOH) were added to the PCR product and centrifuged for 45 min at 3220 x g and room temperature (RT). Afterwards the supernatant was discarded and probes were washed with 100 µl 70 % EtOH and underwent

another centrifugation step for 10 min at 3220 x g and RT. This washing step was performed twice and after the supernatant was discarded tubes were centrifuged upside down on a paper towel for 1 min at 600 x g and RT to remove residual ethanol. Then purified DNA was resuspended in 15µl H_2O and gently mixed for 30 min on a vortexer.

2.3.2 Agarose gel electrophoresis

Agarose gel electrophoresis was used to analyze the amplification of the desired PCR product. This method allows to separate DNA/RNA by length via application of an electric field, which moves the negatively charged nucleic acids through an agarose gel towards the positive electrode. Thereby short fragments move faster through the gel matrix than long fragments.

To prepare a 2 % agarose gel 4 g of SeaKem®LE Agarose (Lonza, Basel, Switzerland) were solved in 200 ml 0,5 x TBE buffer (45mM Tris Base, 45mM Boric Acid and 10mM EDTA in H_2O) and boiled up by microwave heating. To later stain the DNA 8 µl Midori Green Advance (Biozym, Vienna, Austria) were added to the slightly cooled down solution and then it was poured into a gel tray with matching combs to generate the needed number of wells. After the gel solidified it was loaded with 5µl of the PCR products and 5µl Gene Ruler DNA Ladder Mix (Life Technologies (Thermo Fisher Scientific), Waltham, USA) served as size marker. Gel electrophoresis was carried out at 200 V for 30 min and afterwards DNA bands were detected using an UV gel documentation chamber (V029119, Vilber Lourmat, Eberhardzell, Germany) and correct product size was analyzed with the help of the size marker.

2.3.3 Sanger sequencing

To analyze the DNA sequences on a nucleotide level Sanger sequencing was performed. This standard method uses the incorporation of labeled di-deoxynucleotidetriphosphates in a PCR which leads to a chain termination. Afterwards the fluorescent labels can be detected on an automated sequencing machine and thus the exact nucleotide sequence can be identified.

Therefore, the sequencing PCR was performed using the purified DNA of the respective amplification PCR as described in 2.3.1. For pipetting the master mix ddH_2O, 5 x Colorless GoTaq Reaction Buffer (Promega, Madison, USA), BigDye® Terminator v3.1 Cycle (Life Technologies GmbH, Darmstadt, Germany), primers and the purified PCR product were mixed as shown in Table 4. Hereby the reverse and forward primers were used in separate reactions. Then sequencing PCR was performed following the protocol shown in Table 5.

Table 4: Master mix for standard sequencing PCR

Components	**Volume [µl]**
dd H_2O	2,65
Big Dye v3.1	0,7
5x Buffer	1,65
Primer (10 pmol/µl) (Fw or Rv)	1
Purified PCR Product	4
Total	**10**

Table 5: PCR program for standard sequencing PCR

Step	**Temperature (°C)**	**Time**	**Cycles**
Preheating	94 °C	1 min	
Denaturation	94 °C	10 sec	30x
Annealing	50 °C	5 sec (T_A)	
Elongation	60 °C	4 min	
Cooling	10 °C	forever	

PCR products were purified as after the amplification PCR with the difference that this time only 30µl NaAc/EtOH were used and the washing step with 70% EtOH was only performed once. Purified DNA was diluted in 15µl H_2O and gently mixed for 30 min on a vortexer covered with aluminum foil.

For final sequencing 7µl of purified DNA were mixed with 15 µl formamide (Life Technologies (Thermo Fisher Scientific), Waltham, USA) in a 96-well

sequencing plate. Sanger sequencing was performed on a Genetic Analyzer 3130xl (Applied Biosystems, Foster City, USA) and afterwards DNA sequences were processed using the SeqA6 Sample manager software (Applied Biosystems) and PreGap4 and viewed by Gap4 (Staden Package, Open source).

2.3.4 Segregation analysis

Segregation analysis was performed by sequencing the DNA from as many family members as available (in this special case two healthy parents and two affected siblings). According to the families' clinical phenotypes a pedigree was created and following the Mendelian rules the most likely underlying mode of inheritance was determined. Afterwards the sequencing results of all candidate variants were validated upon the family members to minimize the remaining strong candidates as much as possible.

2.4 Investigation of Splice-Variant

2.4.1 RNA isolation of PAXgene and Fibroblasts

Since the remaining intronic candidate variant was predicted to have effects on splicing, presence of aberrant transcripts was confirmed. Therefore, RNA from one patient and healthy controls was isolated from blood cells using the PAXgene Blood RNA Kit (Qiagen, Venlo, Netherlands) and from Fibroblasts using the High Pure RNA Isolation Kit (Roche, Rotkreuz, Swiss). All steps were performed according to the respective manufacturer´s protocol and isolated RNA was eluted in 25 - 40 µl of the appropriate elution buffer and stored at - 80 °C. For determination of RNA concentration, a Spectrophotometer (NanoDrop ND1000, Peqlab Biotechnology, Erlangen, Germany) was used.

2.4.2 cDNA generation with Transcriptor High Fidelity cDNA Synthesis Kit

To further validate the presence of aberrant transcripts the RNA underwent reverse transcription to create cDNA. For this the Transcriptor High Fidelity cDNA Synthesis Kit (Roche, Rotkreuz, Swiss) was used according to the manufacturer's protocol. All reagents were kept on ice.

In a first step the isolated RNA was mixed with random hexamer primers and PCR-grade water to a template-primer mix (Table 6) which was incubated at 65 °C for 10 min to denature secondary structures of the RNA. Random hexamer primers were used to ensure that the resulting cDNA is a complete copy of the expressed mRNA transcripts present in the cell at the time of RNA isolation, which allows subsequent quantitative analysis.

Table 6: Template-primer mix for cDNA Synthesis

Components	**Volume [µl]**	**Final Concentration**
Total RNA	variable	500 ng
Random Hexamer Primer (600pmol/µl)	2 µl	60 µM
H_2O (PCR Grade)	variable	
Total	**11,4 µl**	

Afterwards 8,6 µl of the Reverse-Transcriptase mix, containing 5 x buffer, protector RNase Inhibitor, Deoxynucleotides, DTT, and Reverse Transcriptase as listed in Table 7 were pipetted to the template-primer mix and followed by a two-step amplification protocol including 10 min incubation at 29 °C and 1 h at 48 °C.

Table 7: Reverse-Transcriptase Mix for cDNA Synthesis

Components	**Volume [µl]**	**Final Concentration**
Transcriptor High Fidelity Reverse Transcriptase Reaction Buffer (5 x)	4	1 x (8 mM $MgCl_2$)
Protector RNase Inhibitor (40 U/µl)	0,5	20 U
Deoxynucleotide Mix (10 mM each)	2	Je 1 mM each
DTT	1	5 mM
Transcriptor High Fidelity Reverse Transcriptase	1,1	10 U
Total	**8,6 µl**	

A final incubation step of 5 min at 85 °C which leads to the inactivation of the transcriptase was performed and then the cDNA was stored at -20 °C or used for further applications as amplification or qPCR.

2.4.3 Validation of aberrant transcripts via PCR

To verify the presence of aberrant transcripts the generated cDNA was evaluated using PCR amplification. To ensure that only cDNA was amplified an exon-boundary spanning forward primer was designed which prevents the amplification of genomic DNA. Then reverse primers fitting to the forward primer were designed downstream the mutation with the predicted splice effect in Intron 6 and Exon 7 to cover all possible splice effects through PCR amplification. Amplified transcripts were detected via gel electrophoresis and analyzed by length. The chosen primers are shown in Table 8.

Table 8: PCR primer for validation of aberrant transcripts

Name	**Primer sequences (5'-3')**	**Product length**
RNF170_Exon3/4_Fw	CTTCAAACAGAACAGGATGCAC	See below
RNF170_Exon7_Rv	AACATCCAGAAAAGGCCCCC	395 bp
RNF170_Intron6_Rv	TGGCAGCAATGAAGGTAAAAACT	830 bp

Standard PCR was performed as described in 2.3.1 with the only difference that elongation time was increased to 1 min according to the expected product length. Then samples underwent gel electrophoresis as described in 2.3.2.

2.4.4 Purification of DNA from Agarose Gel

To finally analyze the occurring aberrant transcripts by sequencing, the DNA bands were cut out of the agarose gel using a fluorescent table and purified following the protocol of the QIAquick® Gel Extraction Kit (Qiagen, Venlo, Netherlands).

For this the gel slices were placed in 1,5 ml tubes and 300 µl buffer QG were added. The tubes were incubated for 10 min at 50 °C on a shaker to dissolve the gel slices. Then 100 µl of Isopropanol were added and the solution was pipetted on an QIAquick column placed on a 2 ml collection tube, and centrifuged for 1 min at 17900 x g. Afterwards the flow-through was discarded, the column was replaced in the same collection tube and two washing steps were performed. Therefore first 500 µl buffer QG were added, columns were centrifuged as previously described and flow-through was discarded as before. The same procedure was performed with 650 µl buffer PE with the only difference that the buffer incubation time was increased to 5 min before centrifugation.

To remove residual wash buffer another centrifugation for 1 min at 17900 x g followed before the column was placed into a Clean 1,5 ml tube. In the final step 30 µl of elution buffer (EB) were pipetted on the column and after 4 min incubation for maximal DNA yield the sample was centrifuged to elute the purified DNA.

Afterwards the eluted DNA was Sanger sequenced as described in 2.3.3.

2.4.5 Quantitative RT-PCR with the LightCycler® 480

Quantitative real time PCR was performed on a LightCycler® 480 (Roche, Rotkreuz, Swiss) using the LightCycler® 480 SYBR Green I Master Kit (Roche, Rotkreuz, Swiss). The underlying principle is based on the SYBR Green dye, which is part of the Master mix and emits fluorescence only if it's bound to dsDNA.

This leads to an increase of fluorescence proportionally to the amount of synthetized DNA which allows the analysis of expression levels of single genes by measuring the amount of their coding transcripts.

Therefore, two specific primers amplifying the transcript coding for the gene of interest (RNF170) and three reference genes (RNF111, RNF10, RPLP0) were used which allows further relative quantification. Primers are shown in Table 9.

Table 9: Primer for quantitative RT-PCR

Name	**Primer sequences (5'-3')**
RNF111_qPCR_F+R	F: GCAGAATGCAGCAGAAGTTG R: CCATTCTTGCAGAAGTGGTTG
RNF10_qPCR_F+R	F: CACCCACTGCCAGTCAGGGC R: TCCCCGTCGCTGTCCACAGG
RPLP0_qPCR_F+R	F: CCCGAGAAGACCTCCTTTTT R: GGGTTGTAGATGCTGCCATT
RNF170_qPCR2_F+R	F: GGCAGTTGTGGTCAGTTTCG R: CAGGTGCATCCTGTTCTGTTTG
RNF170_qPCR3_F+R	F: ACTTGTGGCAGTTGTGGTCA R: CAGGTGCATCCTGTTCTGTT

To perform the analysis 2 x Master mix, and PCR grade H_2O from the kit were mixed with the different primers as shown in Table 10 and pipetted into a suitable multi-well-plate. Then cDNA was diluted 1:10 and added to each well in technical triplicates of the analyzed samples and standards.

Table 10: Master mix for quantitative RT-PCR

Components	**Volume [µl]**
H_2O (PCR Grade)	4,5
PCR Primer (each 10µM)	1,5
Master Mix (2x)	7,5
cDNA Template (1:10 in ddH_2O)	1,5
Total	**15**

Afterwards the multi-well-plate was tightly occluded with an adhesive foil and quantification was performed following the automated PCR program of the LightCycler® 480 shown in Table 11.

Table 11: LightCycler® 480 protocol for q RT-PCR

qPCR steps	Temperature [°C]	Time	Cycles
Pre-Incubation	95 °C	5 min	
Amplification 1:			
Denaturation	95 °C	30 s	10x -0,5 °C per cycle
Annealing	64 °C	30 s	
Extension	72 °C	30 s	
Amplification 2:			
Denaturation	95 °C	30 s	40x
Annealing	55 °C	30 s	
Extension	72 °C	30 s	
Melting Curve:	95 °C 62 °C 62 °C → 97 °C	5 s 1 min	+ 0,08 °C per second
Cooling	40 °C	10 s	

Finally, evaluation was carried out with the Light Cycler 480 Software 1.5.1.62 (Roche, Rotkreuz, Swiss) using the standard curve and the reference genes for an advanced relative quantification.

2.5 Cell culture

Fibroblast lines were established from skin biopsies using standard procedures.

2.5.1 Culturing of Fibroblasts

Fibroblasts were cultured in DMEM (Thermo Scientific, Waltham, MA/USA) supplemented with 10% FBS (Thermo Scientific,Waltham, MA/USA) at 37°C and 5% CO_2 (Incubator Heracell 240, Heraeus, Hanau, Germany) in cell culture flasks (25 cm_2 and 75 cm_2) or Plates (57 cm_2). Every four days the medium was replaced (for 25 cm^2 flasks - 3 ml media; for 75 cm^2 and 57 cm^2 - 10 ml) and after reaching the desired confluence cells were split or harvested for further biochemical analyses. For splitting the cells by trypsinization medium was

aspirated and cells were washed once with PBS (Sigma life science, St. Louis, MA/USA). Afterwards Trypsin (Biochrom GmbH, Berlin, Germany) (for 25 cm^2 flasks - 1 ml; for 75 cm^2 - 3 ml) was added and cells were incubated for 2 - 5 min until all cells were in suspension. To stop the reaction the same amount of DMEM was added and cell suspension was dispensed into new flasks (1:2 or 1:3).

2.5.2 Bradykinin treatment

Bradykinin is a peptide that acts as an intracellular messenger in fibroblasts and stimulates the formation and release of IP3 (McAllister *et al.*, 1993) which leads to activation of IP3R´s and their consecutive degradation upon activation (Lu *et al.*, 2011). This treatment was performed to evaluate the effect of a possible IP3R accumulation upon bradykinin stimulation in fibroblasts suggesting that loss of RNF170 harms ubiquitination and proteasomal degradation of IP3R´s.

First, the media was heated up to 37°C in a water bath. Prior to treatment with bradykinin fibroblasts underwent an 4h serum starvation. For this purpose, medium was aspirated, cells were washed 3 times with PBS (Sigma life science, St. Louis, MA/USA) and cultured in DMEM (Thermo Scientific, Waltham, MA/USA) without FBS (Thermo Scientific, Waltham, MA/USA) for 4 hours.

Afterwards treatment media containing 300nm Bradykinin (B3259, Sigma life science, St. Louis, MA/USA, (powder dissolved in ddH_2O and stored as a 300µM stock solution)) was prepared as shown in Table 12 and every cell line was treated for 0 min, 30 min or 60 min respectively.

Table 12: Bradykinin treatment mix (300 nm) for 75cm^2 and 57cm^2 growth area

Bradykinin stock solution (in dd H_20)	**300µM**
DMEM volume	5 ml
Bradykinin stock volume	5 µl
Final volume	5 ml

After treatment cells were harvested and lysed for further western blot analysis as described in 2.5.3 and 2.6.1.

2.5.3 Harvesting cells

To collect cells for further biochemical analyses cells were washed two times with PBS (Sigma life science, St. Louis, MA/USA) and either directly scrapped (Cell-scraper, Sarstedt, Nümbrecht, Germany) in lysis buffer or pelletized. To pelletize cells they were detached by trypsinization as described in 2.5.1 and transferred into a 15 ml Tube. After centrifugation (Centrifuge 5810R/5425, Eppendorf AG, Hamburg, Germany) at 300 x g for 5 min the supernatant was removed and the cell pellet was directly lysed or stored at -80°C.

2.6 Protein biochemical methods

2.6.1 Protein isolation from cultured cells

For protein extraction cell pellets were either resuspended in 200µl RIPA lysis buffer (Sigma life science, St. Louis, MA/USA) or cells were directly scrapped in RIPA lysis buffer (for 75cm^2 flasks - 200µl; for 57cm^2 plates - 100µl) with a Cell-scraper (Sarstedt, Nümbrecht, Germany) and transferred into a 1,5 ml tube. In order to prevent the proteins from proteolytic degradation a proteinase inhibitor cocktail (cOmplete Mini, Roche, Rotkreuz, Swiss) was freshly added to lysis buffer before use. Afterwards samples were incubated on ice for 30 min, vortexing every 5 min and centrifuged at 4°C at 20000xg for 30 min. Finally, the protein containing supernatant was transferred to a clean tube and stored at -80°C. To prevent the lysates from multiple freezing-thawing cycles each sample was divided in several aliquots.

2.6.2 Quantification of Protein Concentration via BCA assay

The BCA assay is a common method to measure the concentration of total protein in a solution by colorimetric detection. The underlying mechanism contains two well - established chemical reactions. First one is the biuret reaction, the reduction of Cu^{2+} to Cu^{1+} by protein in an alkaline medium. Second one is the highly specific chelation of two molecules bicinchoninic acid (BCA)

with one of the reduced Cu^{1+} molecules leading to a purple-colored reaction product with strong absorbance at 562nm which is used for colorimetric detection. The measured absorbance is almost linear with increasing protein concentrations over a wide range (20 to 2000 µg/ml).

To determine the concentration of a sample with this assay, a protein standard curve with known protein concentrations is required and for that bovine serum albumin (BSA) was used as protein standard and the serial dilution in PBS (Sigma life science, St. Louis, MA/USA) was prepared following the manufacturers protocol. The resulting concentration of protein standards is shown in Table 13.

Table 13: BSA serial dilution in PBS for BCA assay protein standard curve

Vial	Final BSA Concentration (µg/ml)
A	2000
B	1500
C	1000
D	750
E	500
F	250
G	125
H	25
I	0 = blank

Except the PBS (Sigma life science, St. Louis, MA/USA) all applied reagents were included in the Pierce BCA Protein Assay Kit (Thermo Scientific, Waltham, MA/USA) and used according to the manufacturers protocol.

To perform this assay, the protein sample was pre-diluted 1:10 in PBS (Sigma life science, St. Louis, MA/USA) and the BCA working reagent was prepared via mixing reagent A and reagent B from the Kit in a 50:1 ratio.

The protein standards and the diluted samples were pipetted in triplicates of 10µl each on a 96-well plate. Afterwards 200µl of the BCA working reagent was added per well and the plate was incubated at 37°C for 30 min. Then the absorbance was measured at 595 nm with the iMark™ Microplate Absorbance Reader (Bio-Rad Laboratories, Hercules, CA/USA) and the Microplate Manager® 6 Software (Bio-Rad Laboratories, Hercules, CA/USA) and protein concentration was determined accordingly to the standard curve.

2.6.3 Immunoblotting

Immunoblotting was performed to detect proteins of interest on a protein - binding membrane using specific antibodies.

In the first step the proteins need to be separated by size. Therefore, a SDS polyacrylamide gel electrophoresis (PAGE) was performed. To ensure the correct size classification of proteins they need to be linearized using heat denaturation and the reducing agent DTT for sample preparation. Furthermore, the addition of SDS to the samples leads to an equal distribution of negative charge according to the molecular weight which allows the size - dependent separation of proteins in an electric field.

For sample preparation 40 µg of the protein lysates extracted as described in 2.6.1 were diluted in 5X Pierce™ Lane Marker Reducing Sample Buffer (5:1 Thermo Scientific, Waltham, MA/USA) and 10X DTT (10:1 Thermo Scientific, Waltham, MA/USA) and ddH_2O was added to reach equal loading volumes. Then the whole samples were boiled at 95°C for 5min in the T100 ™ Thermal Cycler (Bio-Rad Laboratories, Hercules, USA) to perform the heat denaturation and cooled down to 4°C until loading.

Bis-Tris SDS gel preparation was performed with the help of a Mini Protean® Casting Module (Bio-Rad, Hercules, CA/USA). At first the glass plates were cleaned with 70% Ethanol and the gel cassette was assembled in the casting stand. Then the separating gel was poured and the pore size was chosen according to the protein size. To separate low molecular weight proteins higher percentage gels are used and vice versa (in this case: 12 % gels for RNF170 (~30 kDA) and 6 % gels for IP3R3 (~300 kDA) immunoblots).

Therefore the 3.5X Bis-Tris buffer (1 M Bis-Tris in ddH2O, pH 6.5), 40% Acrylamide (AppliChem, Darmstadt, Germany) and ddH_2O were mixed in a 15 ml falcon. To start the polymerization of the gel the TEMED (Sigma life science, St. Louis, MA/USA) and APS (Sigma life science, St. Louis, MA/USA) were added and the whole solution was pipetted into the assembled glass plates.
Finally, the separating gel was overlaid with 100% isopropanol to avoid the formation of bubbles within the gel.
After 30 min polymerization, the isopropanol was removed and the stacking gel was prepared the same way, using a 10 x comb to generate the needed number of wells.
The exact amount of components used for the different stacking and separating gels is shown in Table 14.

Table 14: Gel preparation of Bis-Tris SDS gels for electrophoresis

1 gel	**stacking (4%)**	**separating (6%)**	**separating (12%)**
3.5 x Bis-Tris-Buffer, ml	0,86	2,29	2,29
40 % acrylamide, ml	0,3	1,2	2,4
ddH_2O, ml	1,81	4,43	3,23
10 % APS, µl	30	80	80
TEMED, µl	3	8	8
Total volume, ml	**3**	**8**	**8**

After another 30 min polymerization of the stacking gel, the electrophoresis tank (Bio-Rad Laboratories, Hercules, CA/USA) was filled with running buffer (Table 15) and the gel with glass plates was inserted into the tank. Then the comb was carefully removed and the wells were rinsed with running buffer before the samples and size marker were loaded. According to the size of the proteins of interest it was either used 5µl of the Precision Plus Protein™ Dual Color standard (Biorad Laboratories, Hercules, CA/USA) for smaller proteins or 10µl of HighMark™ Pre-Stained Protein Standard (Thermo Scientific, Waltham,

MA/USA) for bigger ones. The gel was run at 120 V for about 80 min until the dye front reached the end of the gel.

Table 15: Preparation of Western Blot solutions

Western Blot solutions	**Compositions**
1X TBS	50mM Tris-base (pH7.4); 150mM NaCl in ddH_2O
1X TBS-T	50mM Tris-base (pH7.4); 150mM NaCl, 0.1% Tween20 (v/v) in ddH_2O
1X running buffer	1M MOPS, 1M Tris-Base, 70mM SDS, 20mM EDTA in ddH_2O
1X transfer buffer	0.25M Bicine, 0,25M Bis-Tris, 20mM EDTA, 10% (v/v) methanol in ddH_2O

* ddH_2O: double-distilled H_2O, EDTA: ethylenediaminetetraacetic acid, MOPS: 3-(N-morpholino) propanesulfonic acid, NaCl: sodium chloride, SDS: sodium dodecyl sulfate

After the electrophoretic separation of the protein samples by size, in a second step the proteins were blotted from the gel on a protein binding membrane which allows analyzing proteins by immunodetection. Therefore, another electrophoresis was performed to transfer the negatively charged proteins from the gel onto a protein- binding membrane.

For this purpose a PVDF membrane (Merck Millipore, Burlington, MA/USA) was used and a blotting sandwich was assembled to obtain a clean and even protein transfer.

The transfer buffer was prepared as shown in Table 15 and both fiber pads and filter pads were equilibrated in transfer buffer for 5 min whilst the PVDF membrane was activated in Methanol for a few seconds and then equilibrated in transfer buffer as well. To assemble the blotting sandwich the gel was carefully taken out of the glass plates used for SDS-PAGE and the membrane was placed on top of the gel. Then filter pads were added on each side and after

striking out possible air bubbles, which would harm the protein transfer from gel to membrane, with an 15ml tube the growing sandwich was clamped tightly in between the fiber pads into a gel holder cassette. Thereafter the cassette was placed in a suitable module inside the electrophoresis tank (Bio-Rad Laboratories, Hercules, CA/USA) which was filled with transfer buffer and a cool pad to maintain even buffer temperature. Subsequently blotting was performed at 350 mA, 100 V and 4 °C for 2h.
For transfer checking the membrane was carefully removed out of the blotting cassette and stained for 5min with Ponceau S solution (Sigma Aldrich, Chemie GmbH, Munich). Afterwards the protein ladder was marked with a pencil and the membrane was cut inside a transparent film to be able to use two different membranes for primary antibody labeling at a time. Then the membrane was washed with VE water and TBS-T to remove the Ponceau staining before the last step was performed.

In the final step, indirect immunodetection was performed to detect the proteins of interest. For this a specific primary antibody which binds selectively to the chosen protein is incubated with the protein binding membrane. Afterwards this primary antibody is recognized by a secondary antibody conjugated to the enzyme horseradish peroxidase whose activity can be imaged by adding a solution which contains chemiluminescent substrates and detecting the resulting enzymatic chemiluminescence.
All following washing or incubation steps were performed on a shaker or roller shaker depending on the kind of vessel used for each step. First the membranes were blocked in TBS-T with 5% non-fat dried milk powder (Sigma Aldrich, Chemie GmbH, Munich) for 1h at RT to prevent non-specific background binding of the antibodies. Then the membranes were incubated overnight at 4°C with the primary antibodies using a 50 ml Falcon. All antibodies were diluted in TBS-T with 5% non-fat dried milk powder (Sigma Aldrich, Chemie GmbH, Munich) except the mouse anti-Vinculin antibody (1:100000, V9131, Sigma life science, St. Louis, MA/USA) which was diluted in TBS-T with 5 % Western Blocking Reagent (Roche, Rotkreuz, Swiss). For detection of

RNF170 a rabbit anti-RNF170 antibody (1:500, HPA054621, Atlas Antibodies, Bromma, Sweden) (shows multiple bands, therefore knockout validated in the lab) was used as primary AB and mouse anti-ß-Actin AB (1:20000, A5441, Sigma life science, St. Louis, MA/USA) served as loading control. For detection of IP3R3 membranes were probed with mouse anti-IP3R-3 AB (1:1000, 610312, BD Biosciences, Franklin Lakes, NJ/USA) and for loading control a mouse anti-Vinculin antibody (1:100000, V9131, Sigma life science, St. Louis, MA/USA) was used.

After overnight incubation, the membranes were washed thrice in TBS-T for 10 min before they were incubated for 1h at RT with the HRP-conjugated secondary antibodies (1:10000, 115-035-003, Peroxidase AffiniPure Goat Anti-Mouse IgG (H+L) and 1:10000, 111-035-003, Peroxidase AffiniPure Goat Anti-Rabbit IgG (H+L), Jackson ImmunoResearch, Cambridgeshire, UK). Afterwards the membranes were once again washed three times with TBS-T and subsequently used for immunodetection.

To visualize the protein bands the detection reagent (ECL; Pierce^{TM} ECL Western Blotting Substrate, Thermo Scientific, Waltham, MA/USA) was prepared by mixing the given reagents 1:1 and pipetted even on the membranes for approximately 1min. Then the membranes were covered into a transparent film and remaining ECL and air bubbles were carefully removed by striking over the plastic film. Then the chemiluminescence was detected with ChemiDoc XRS+ imaging system (Biorad, Munich, Germany) and analyzed with the Image Lab 5.0 software. Exposure time was optimized for the different antibodies and varied between a few seconds up to 2 min.

2.6.4 Quantification of Western Blot

For quantification of the protein levels the Image J software (open source) was used and quantification was carried out through densitometry, a semi-quantitative measurement of optical density.

2.7 Statistical analysis

Statistical analyses were performed with JMP 14.2 Software for Mac.

Results obtained from the quantitative real-time PCR were tested for statistical significance with a two-sided Wilcoxon rank sum test.

For comparison of continuous variables across groups, as the semiquantitative Immunoblots of IP3R-3 levels in fibroblasts, results obtained of the triplicate Immunoblots were statistically evaluated via two-sided Wilcoxon rank sum test as well.

To compare the response to the bradykinin treatment in fibroblasts across patient and controls repeated measures ANOVA was performed.

P-values of $p<0,05$ were considered as statistically significant.

3. Results

3.1 Identification of *RNF170* - a novel disease gene causing HSP

3.1.1 Candidate genes identified via GENESIS in silico analysis

As mentioned above, in this study we aimed at the identification of novel genes causing HSP. Therefore, we applied the step-wise analysis approach described in 2.2 on 142 WES and WGS datasets of patients suffering from genetically unsolved HSP. Here we report one family with autosomal recessive early-onset HSP which we could solve in this study. Therefore, we used WGS data of the two affected siblings and the first analysis step - screening for rare coding variants in 289 genes known to cause HSP revealed no molecular diagnosis. Thus, we went on to the next step and according to the assumed mode of inheritance we filtered the WGS data for potentially biallelic rare coding and splice region variants. We identified five candidate genes shown in Table 16.

Table 16: Candidate genes identified by whole genome sequencing

gene	genomic variant (hg19)	zygosity	cDNA	protein effect	mutation type	gnomAD MAF	PolyPhen	CADD score	segregation supports pathogenicity
DNAH5	chr5:13714683T>C	het	NM_001369.2: c.12956A>G	p.N4319S	missense	0.00001626		25.200	no
DNAH5	chr5:13716802G>A	het	NM_001369.2: c.12706-3C>T	p.?	splice region	0		10.910	
FCRL2	chr1:157737105C>T	het	NM_030764.3: c.1078G>A	p. A360T	missense	0.00002886	0.78	12.890	no
FCRL2	chr1:157738309G>T	het	NM_030764.3: c.778C>A	p. L260M	missense	0.002774	0.951	12.400	
GPR98	chr5:89925235G>T	het	NM_032119.3: c.1718G>T	p. G573V	missense	0.0002925	1.0	18.180	no
GPR98	chr5:90012539G>A	het	NM_032119.3: c.9440G>A	p. R3147Q	missense	0.0003002	0.09	15.960	
RNF170	chr8:42720556T>C	hom	NM_030954.3: c.396+3A>G	p.A109Nfs*9	splice region	0.000004067	N/A	N/A	yes
ZNF646	chr16:31090120C>G	het	NM_014699.3: c.2475C>G	p. D825E	missense	0.0006352	0.347	14.200	no
ZNF646	chr16:31090182G>T	het	NM_014699.3: c.2537G>T	p. G846V	missense	0.0006352	1.000	18.280	

*_DNAH5_: Dynein Axonemal Heavy Chain 5, _FCRL2_: Fc Receptor Like 2, _GPR98_: G-protein coupled receptor 98, _RNF170_: Ring Finger Protein 170, _ZNF 646_: Zink Finger Protein 646; Filter settings: MAF in ExAC and EVS and 1000 Genomes < 1%; pass quality filters (read depth > 8, GQ > 50 OR QUAL > 35), compatible with autosomal recessive inheritance. Allele count in inhouse database (e.g. GENESIS) < 21 in 5900 individuals. Modified from Supplementary Data (Wagner *et al.*, 2019).

3.1.2 Sanger sequencing of the candidates and segregation analysis

To validate the possible candidate genes, Sanger sequencing was performed for all five genes among the two patients and three additional unaffected family members (parents, healthy sibling). Subsequent segregation analysis over the family could exclude four of these genes, as the variants in four candidate genes were located on the same allele (*in cis*; variants in *DNAH5*, *FCRL2*, *GPR98*, *ZNF646*). Interestingly, both variants in *ZNF646* were present in both parents, indicating not only their location *in cis* but also a possible founder effect or distal relationship of the parents. In summary, only *RNF170* remained as a possible disease-causing gene under the selected filtering model. The detailed genotypes of all evaluated family members are shown in Table 17.

Table 17: Sequencing results and segregation analysis of the Index family

genomic variant (hg19)	zygosity	gene	H.1 (father)	H.2 (mother)	H.3 (sister)	H.4 (patient)	H.5 (patient)	segregation supports pathogenicity
			healthy	healthy	healthy	affected	affected	
chr5:13714683T>C	het	*DNAH5*	T/C	T/T	no data	T/C	T/C	**no (excluded in cis, paternal)**
chr5:13716802G>A	het	*DNAH5*	G/A	G/G	G/G	G/A	G/A	
chr1:157737105C>T	het	*FCRL2*	C/T	C/C	C/C	C/T	C/T	**no (excluded in cis, paternal)**
chr1:157738309G>T	het	*FCRL2*	G/T	G/G	G/G	G/T	G/T	
chr5:89925235G>T	het	*GPR98*	G/G	G/T	no data	G/T	G/T	**no (excluded in cis, maternal)**
chr5:90012539G>A	het	*GPR98*	G/G	G/A	no data	G/A	G/A	
chr8:42720556T>C	hom	RNF170	T/C	T/C	T/C	C/C	C/C	**segregates**
chr16:31090120C>G	het	*ZNF646*	G/T	G/T	no data	G/T	G/T	**no (both parents carry both variants)**
chr16:31090182G>T	het	*ZNF646*	C/G	C/G	no data	C/G	C/G	

*chr: chromosome, T: thymine, C: cytosine , G: guanine, A: adenine, het: heterozygous, hom: homozygous.

With this approach we detected a homozygous *RNF170* mutation in both patients presenting with early childhood onset HSP. The single amino acid exchange mutation c.396+3A>G (chr8:42720556T>C, p.A109Nfs*9) is located at the 3rd base of intron 5-6 in a highly conserved region and was predicted to affect splicing (Berkeley Drosophila Genome Project (REESE *et al.*, 1997)). The variant follows the segregation across the family in an autosomal recessive manner as shown in Figure 4.

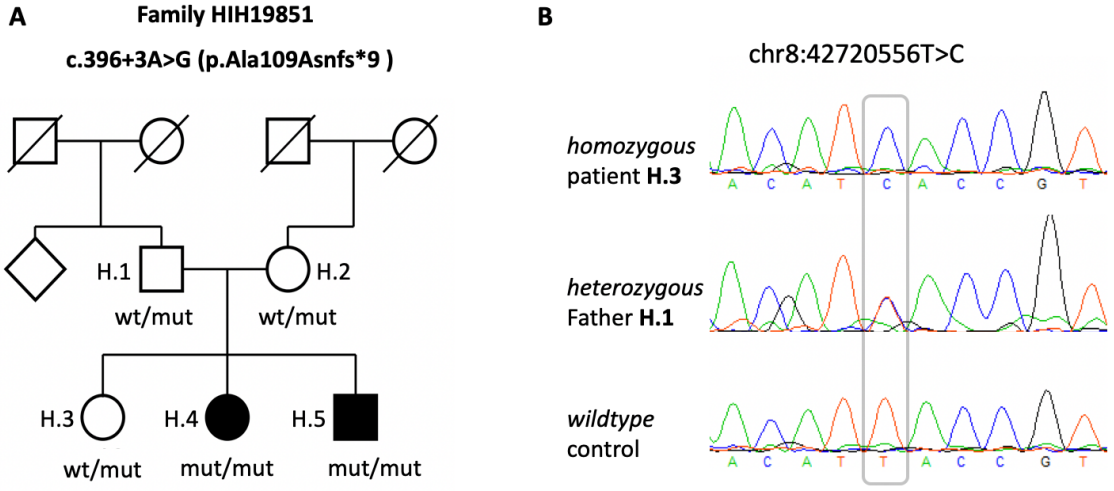

Figure 4: Family tree and segregation analysis of the identified mutation in the RNF170 patients. (A) Pedigree: *Squares: males, circles: females, filled symbols: affected individuals, mut: mutation, wt: wildtype* ***(B)*** *Representative sequencing analysis of RNF170 Intron 5-6 of the homozygous patient H.4, the heterozygous father and a control. The position of the chr8:42720556T>C mutation is marked by a light grey box.*

3.1.3 Validation of the predicted splice effect of the *RNF170* variant

As the remaining candidate variant in *RNF170* segregates with the disease in an autosomal recessive manner, we went on with further investigations of the predicted splicing effect to support the assumed pathogenicity of this intronic variant.

According to Berkeley Drosophila Genome Project (REESE *et al.*, 1997) the homozygous splice region variant c.396+3A>G (NM_030954.3) is predicted to cause a loss of the splice donor site of exon 5. For identification of possible aberrant transcripts we thus generated cDNA by using mRNA derived from patient H.4 blood cells and fibroblasts via RT-PCR. Thereby we could confirm the splice effect as gel electrophoresis of the RT-PCR products showed a shortened transcript in patients tissue in comparison to wildtype transcripts shown in three unaffected controls (Figure 5 A). Further sequencing analysis of the generated cDNA revealed that patients transcript lacked exon 5 (Figure 5 B). Since exon 5 contains 74 bases this aberrant transcript results in a frameshift of the mRNA. This shift of the reading frame was predicted to show a premature stop codon generating a truncated protein (p.Ala109Asnfs*9).

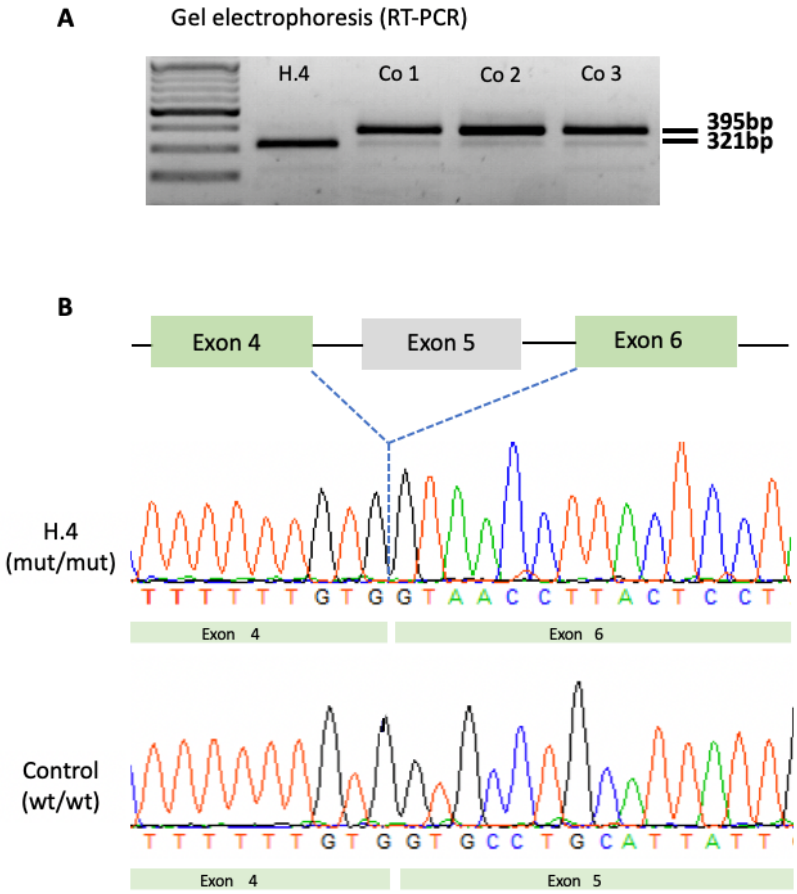

Figure 5: Gel electrophoresis and consecutive Sanger sequencing (A) *Representative agarose gel electrophoresis of blood derived cDNA from patient H.4 and three unaffected controls showed the expression of a shortened transcript in the patient. (estimated length: aberrant transcript: 321bp, wildtype transcript: 395bp), 2 % agarose gel and the Gene Ruler DNA Ladder Mix were used.* ***(B)*** *Consecutive Sanger sequencing showed that the aberrant transcript is lacking exon 5; the dashed lines indicate where exon 5 is lacking in the mutated sequence. mut: mutation, wt: wildtype. Modified from* (Wagner *et al.*, 2019).

3.1.4 Decreased RNF170 expression levels

To further validate the RNF170 expression levels both regarding mRNA and protein expression, quantitative real time PCR and RNF170 western blots were performed.

For quantification of the RNA transcripts, mRNA derived from peripheral blood cells and fibroblasts of patient H.4 and three unaffected control samples were used to generate cDNA. Real-time PCR quantification was performed in relation

to three reference genes (*RNF111*, *RNF10*, *RPLP0*) and showed a significantly reduced *RNF170* expression compared to the controls (Figure 6). The shortened transcript reaches 50 % of normal *RNF170* mRNA expression levels in patient fibroblasts (p=0,0162) and 36 % in patient peripheral blood cells (p=0,0162). This decreased level of *RNF170* gene expression in patient H.4 most likely seems to be caused by partial nonsense mediated RNA decay (NMD) of the aberrant transcript.

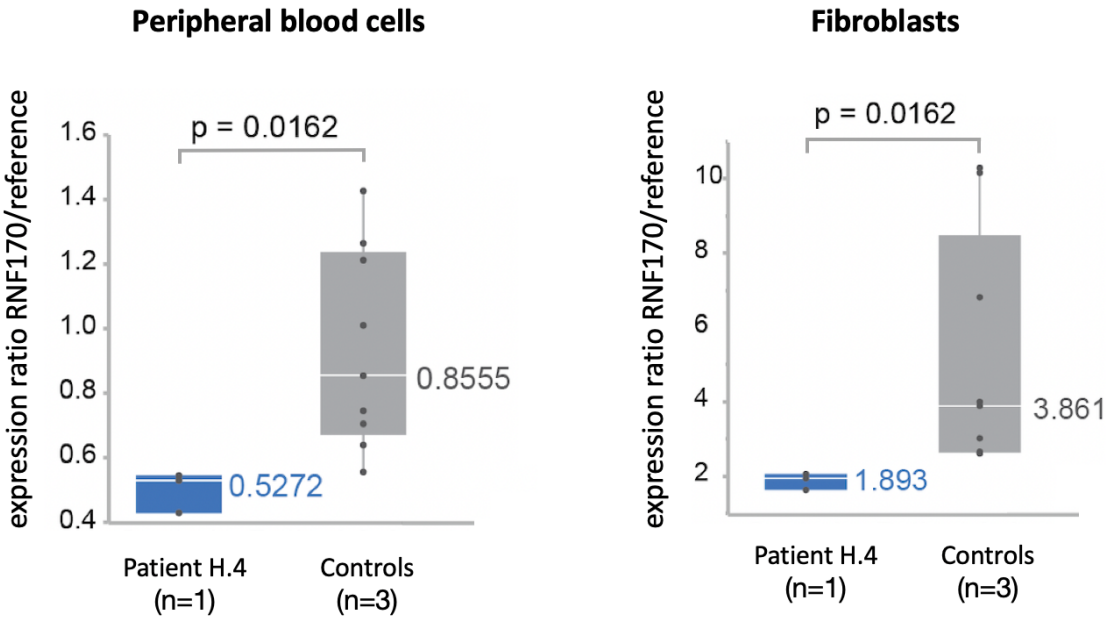

Figure 6: Relative expression level of RNF170 in peripheral blood cells and fibroblasts. *Quantitative real-time PCR from cDNA derived from patient H.4 showed significantly reduced RNF170 expression levels compared to three healthy controls. Modified from* (Wagner *et al.*, 2019).

However, the residual *RNF170* expression in the qPCR suggests that mutant RNA at least partially escapes nonsense mediated RNA decay. We therefore performed a western blot for RNF170 to quantify the protein expression of a possible truncated protein even though this would lack parts of the RING domain and therefore be most likely dysfunctional. Immunoblot analysis was performed on protein extracts of fibroblasts of patient H.4 and one fibroblast control cell line. Using a CRIPSR/Cas9 knockout (KO) validated RNF170

antibody, no RNF170 (25 kDA) expression was detected in patient derived samples compared to the healthy control (Figure 7). The RNF170 knockout cell line used for validation was generated by a master student in the lab.

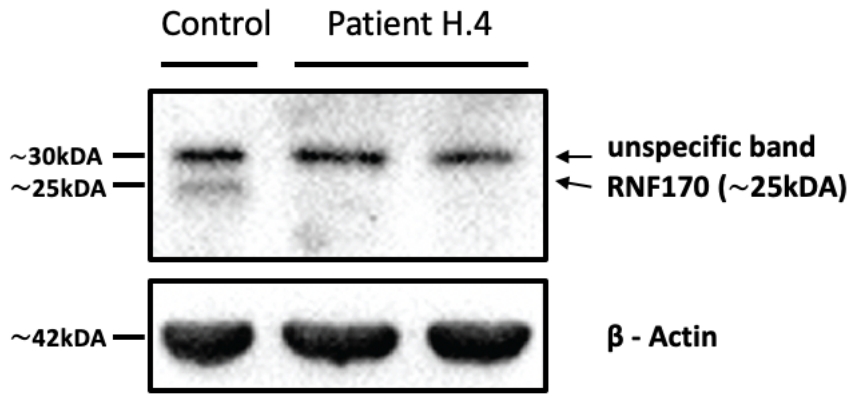

Figure 7: RNF170 protein expression level in patient H.4 fibroblasts and a fibroblast control line. *Western blot analysis shows no residual RNF170 expression in two protein extractions of patient H.4 fibroblasts. Lower arrow marks the height of the specific 25kDA band representing RNF170. Upper arrow marks an unspecific band misleadingly stained by the RNF170 antibody (KO validated RNF170 AB was used). β-Actin was used as a loading control. Modified from* (Wagner *et al.*, 2019)*.*

3.2 Identification of additional families carrying *RNF170* variants

3.2.1 Gene matcher results

In order to identify additional families carrying biallelic loss-of-function mutations in *RNF170* which would strengthen the causal relationship between *RNF170* mutations and the HSP phenotype, we performed a web search using the GeneMatcher collaboration platform. Hereby we used the index patient H.4 from family HIH 19851 for matchmaking and identified three more unrelated families with biallelic mutations in *RNF170*. All families identified via GeneMatcher also manifested with an HSP phenotype.

3.2.2 *RNF170* variants identified in three more families

RNF170 variants in the three additional families where identified by Whole Exome sequencing by collaborators. All of these families demonstrated a

consanguinity of the parents and affected family members suffered neurological symptoms representing an HSP phenotype. According to the respective pedigrees (shown in Figure 8) an autosomal recessive mode of inheritance was assumed and that is why WES data was filtered for potentially biallelic variants leading to selection of *RNF170* as potential candidate gene in all these families.

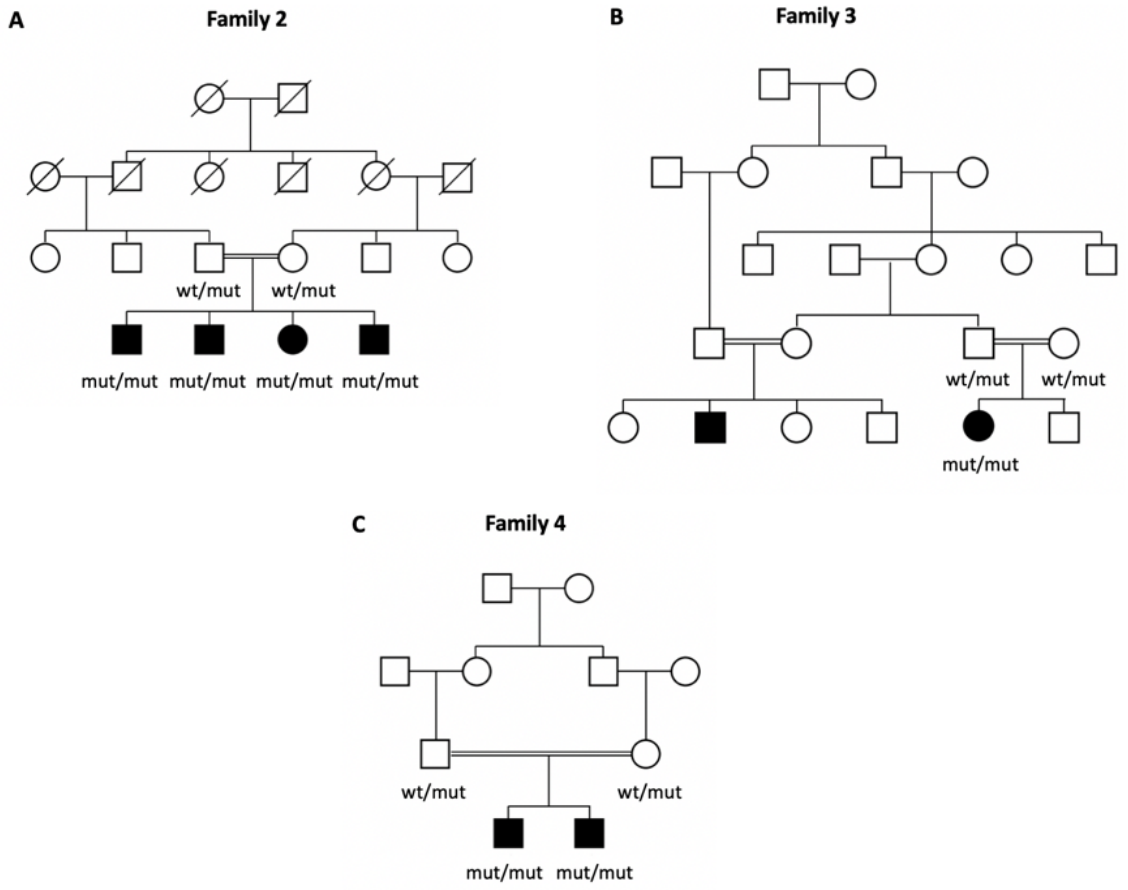

Figure 8: Pedigrees and segregation analysis of the identified RNF170 mutations in additional families. (A - C) Pedigrees of families 2 - 4: *Squares: males, circles: females, filled symbols: affected individuals, double line: consanguinity, mut: mutation, wt: wildtype. Pedigrees extracted with modifications from Figure 1* (Wagner *et al.*, 2019).

In the first additional family (Family 2), an Iranian family with four siblings suffering from HSP, a homozygous missense variant (c.304T>C, p.Cys102Arg) could be detected amongst all affected individuals, whilst parents showed an heterozygous genotype which supports segregation across the family.

Pathogenic relevance of this variant is strengthened by the fact, that mutation of the respective cysteine102 has already been shown to compromise the RNF170 ligase activity in vitro (Lu *et al.*, 2011).

In the second family (Family 3), a consanguineous Tunisian family with one affected child, analysis of copy number variations between the patient and both parents revealed a homozygous intragenic *RNF170* deletion of exons 4 – 7 (breakpoint PCR and sequencing identified the accurate mutation as chr8:g.42,704,626_42,729,012delinsTTTTGGT). This leads to loss of two of the three transmembrane domains as well as complete loss of the important RING domain.

In the last Iranian family (Family 4) the two affected individuals showed a homozygous deletion of adenine and guanine (c.518_519delAG) which results in a frame-shift and thus generates a premature stop codon (p.Arg173Asnfs*49). This would lead to a truncated protein lacking two out of three transmembrane domains if protein expression is not terminated before, due to nonsense mediated RNA decay.

All *RNF170* mutations among families including the index family are summed up in Table 18.

Table 18: RNF170 variants identified in four families segregating with HSP phenotype

family	genomic variant (hg19)	zygosity	cDNA	protein effect	mutation type	gnomAD alleles
Index	chr8:42720556T>C	hom	NM_030954.3: c.396+3A>G	p.Ala109Asnfs*9	splice	1/245854
2	chr8:42725165A>G	hom	NM_030954.3: c.304T>C	p.Cys102Arg	missense	1/246108
3	chr8:42704626_42729012delinsTTTTGGT	hom	c.? [delEx4_7]	p.?	CNV	absent
4	chr8:42711560_42711561delTC	hom	NM_030954.3: c.518_519delAG	p.Arg173Asnfs*49	deletion	absent

*chr: chromosome, T: thymine, C: cytosine, G: guanine, A: adenine, del: deletion, ins: insertion, hom: homozygous, RNF170: Ring Finger Protein 170,

Ala: alanin, Asn: asparagine, Cys: cysteine, Arg: arginine, CNV: copy number variation, gnomAD: Genome Aggregation Database. Modified from Supplementary Data (Wagner *et al.*, 2019).

3.2.3 Clinical phenotype of RNF170 families

Our index patient H.4 is a 53-year-old female and the second child of apparently unrelated parents, both originating from the same small village in Germany. Pregnancy and delivery were uneventful. The early psychomotor development was regular and the motor milestones were reached on time. At the age of 4 years she first developed a gait abnormality and started walking on tiptoes. From then on her spastic gait disturbance worsened slowly. At age 16 she received Achilles tendon surgery on both sides to reduce spasticity. Approximately at the age of 20 years she lost independent walking and depended on walking aids. At 53 years her maximum ability to walk was reduced to 100 m with walking aids, while longer distances required the use of a wheelchair. She showed no cognitive impairment and finished her education to become a bank clerk after school.

She suffers urinary urge incontinence, which is why she is permanently dependent on wearing pads.

The patient has one younger brother suffering from neurological symptoms consistent with the diagnosis of complicated HSP as well and one older sister without neurological diseases. Both parents are healthy and alive. The patient is married and has no children.

Neurological examination of the index patient at the age of 53 years showed slight saccadic pursuit and mild upper limb ataxia with intention tremor on the right side. Furthermore, the patient suffered a mild cervical dystonia. Examination of the upper limb showed slightly reduced fine motor skills predominantly on the right side, brisk upper limb reflexes on both sides and increased spastic tone in the elbow flexion (° 0–1 on the Ashworth scale). Examination of the lower limb showed lower limb weakness for hip abduction (~4/5 on the MRC scale), moderate spastic paraplegia with adductor and knee extensor spasticity (° 1–2 on the Ashworth scale), brisk tendon reflexes with

cloni and positive Babinski sign. There were contractures in hip adduction and ankle flexion (after surgery). Senses of touch, joint position, vibration and temperature were intact. Aided walking was predominantly spastic with narrow gait base.

Nerve conduction studies indicated an axonal sensorymotor peripheral neuropathy. Sensory evoked potentials (done at age 30) showed no cortical potential for the lower limbs which indicates a subclinical involvement of the central sensory tracts. Motor evoked potentials, visually evoked potentials and brain MRI have not been performed.

According to this reported case the patient´s phenotype can be classified as early - onset complicated HSP. Also her younger affected brother, who carries the same *RNF170* mutation as the index patient, showed very similar neurological findings.

In summary, our two patients, as well as the seven affected individuals from three more unrelated families who underwent detailed clinical examination, showed early-onset lower limb predominant spastic paraparesis with mild upper limb involvement later in disease and several variably complicating factors. This indicates that RNF170-associated disease often presents with a phenotype of early-onset complicated HSP often accompanied by optic atrophy and variably observed other complicating symptoms that affect other parts of the central nervous system e.g. cerebellum.

All detailed clinical information of the nine examined patients are shown in Table 19.

Table 19: Clinical information of patients with homozygous RNF170 mutations

family	**HIH19851**		**Family 2**				**Family 3**	**Family 4**	
patient	**H.4**	**H.5**	**patient 1**	**patient 2**	**patient 3**	**patient 4**	**patient 2**	**patient 1**	**patient 2**
mutation	Ala109Asnfs*9 (hom)	Ala109Asnfs*9 (hom)	Cys102Arg (hom)	Cys102Arg (hom)	Cys102Arg (hom)	Cys102Arg (hom)	delEx4_7 (hom)	Arg173Asnfs*49 (hom)	Arg173Asnfs*49 (hom)
moi / gender	AR/F	AR/M	AR/M	AR/M	AR/F	AR/M	AR/F	AR/M	AR/M
race/origin	Germany	Germany	Iran	Iran	Iran	Iran	Tunisia	Iran	Iran
age at onset (y)	3	5	2	2	2	2	2	3	3
age at exam (y)	53	34	12	11	7	4	4	17	23
age at loss of independent walking	20	22	11.5	still walking	still walking	still walking	still walking	still walking	still walking
delayed motor development	-	-	+	+	+	+	+	-	-
cognitive deficits	-	-	-	-	-	-	-	-	-
visual system	mild optic atrophy	n. d.	severe optic atrophy	moderate optic atrophy	mild optic atrophy	mild optic atrophy	not examined	optic atrophy	optic atrophy
oculomotor abnormalities	saccadic pursuit	saccadic pursuit	-	-	-	-	-	saccadic pursuit	saccadic pursuit
dysarthria/ dysphagia	-/-	-/-	+/+	+/+	+/-	+/-	-/-	+/-	+/-
UL/LL spasticity	+/+	+/+	-/+	-/+	-/+	-/+	-/+	+/+	+/+
UL/LL tendon reflexes	brisk/brisk	brisk/brisk	normal/brisk	normal/brisk	normal/brisk	normal/brisk	normal/brisk	brisk/brisk	brisk/brisk

UL/LL weakness	-/+ (proximal)	-/+ (proximal)	-/+ (distal)	-/+ (distal)	-/-	-/-	-/+	-/+	-/+
muscle atrophy	-	-	+ (generalized, severe)	-	-	-	-	-	-
extensor plantar response	+	+	+	+	+	+	-	+	+
sensory deficits**	-/-/-/-	+/-/+/+	-/-/-/-	-/-/-/-	-/-/-/-	-/-/-/-	-/-/-/-	-/-/-/-	-/-/-/-
ataxia	-	-	+ (upper limb and gait)	+ (upper limb and gait)	+	+	-	+	+
extrapyramidal involvement	mild cervical dystonia	-	-	-	-	-	-	-	-
urinary/fecal urgency or incontinence	+/-	+/-	-/-	-/-	-/-	-/-	-/-	-/-	-/-
nerve conduction studies	axonal polyneuropathy	axonal polyneuropathy	normal	normal	n.d.	n.d.	normal	normal	normal
motor evoked potentials	n.d.	UL normal, LL reduced cortical amplitudes	n.d.	n.d.	n.d.	n.d.	n.d.	n.d	n.d
sensory evoked potentials	LL no cortical potential (age 30)	UL prolonged central latency, LL no cortical potential (age	n.d.	n.d.	n.d.	n.d.	normal	n.d	n.d

		33)							
visually evoked potentials	n.d.	n.d.	normal	normal	normal	n.d.	n.d.	increased p100 latency and reduced amplitude	increased p100 latency and reduced amplitude
MRI	n.d.	cranium and cervical spine normal	significant cerebellar atrophy	cerebellar atrophy	normal	n.d.	cranium and cervical spine normal	normal	normal

*moi: mode of inheritance, AR: autosomal recessive, M: male, F: female, hom: homozygous, het: heterozygous, UL: upper limb; LL: lower limb; y: years, n.d.: not done, **vibration/joint position/surface/temperature. Adapted from (Wagner *et al.*, 2019).

3.3 Mutations in RNF170 result in accumulation of IP3R3

3.3.1 Accumulation of IP3R3 in native Western Blots

To test the loss-of-function hypothesis of the identified RNF170 mutation, we performed further protein biochemical analyses to gain functional evidence for the cellular mechanism and pathogenic relevance of RNF170 deficiency.

RNF170 operates as an E3 ubiquitin ligase which conjugates ubiquitin molecules to IP3R´s leading to their degradation via the Ubiquitin Proteasome Pathway. According to this pre-known data we hypothesized that loss of RNF170 results in reduced ubiquitination and proteasomal degradation of IP3R, causing an accumulation of IP3R in patient cells. Since the IP3R3 subtype is the main isoform in human fibroblasts an antibody specific for this subtype was used. As shown in Figure 9 we could demonstrate that basal IP3R3 levels were increased approximately 4-fold in patient H.4´s fibroblasts compared to four unrelated healthy control cell lines (p values for pairwise comparisons: p_1=0,0004, p_2=0,0027, p_3=0,0008, p_4=0,0006).

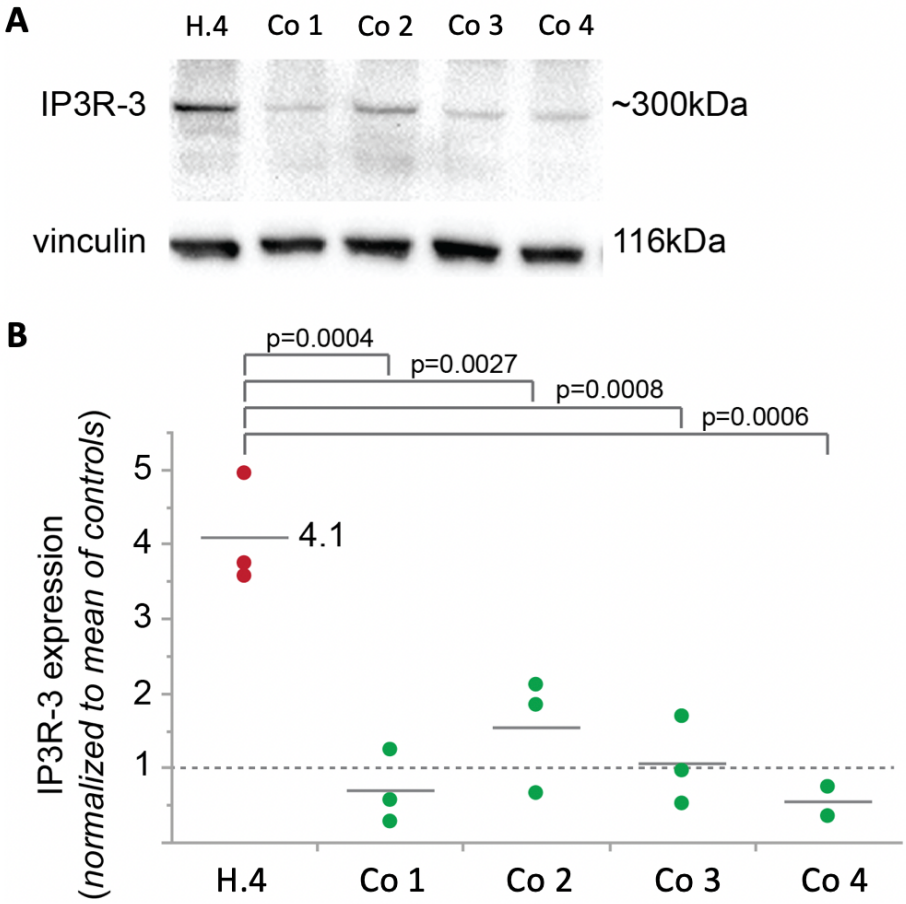

Figure 9: IP3R3 protein expression level in patient H.4 fibroblasts and four fibroblast control lines. (A) *Western blot analysis of IP3R3 shows increased expression levels in patient H.4 compared to four controls caused by a loss of RNF170 which results in decreased IP3R3 degradation. Western blots from a representative experiment are shown. Vinculin was used as a loading control.* ***(B)*** *Semiquantitative immunoblot analysis shows significantly increased (Wilcoxon rank sum test, 2-sided) IP3R3 expression. Horizontal lines represent medians. Dots represent single data points. All results (except for Co 4 (n=2)) were obtained of three technical replicates. Modified from* (Wagner *et al.*, 2019).

3.3.2 Abolished degradation of IP3R3 under bradykinin stimulation

To additionally investigate the RNF170 ligase effects under stimulated conditions we performed a bradykinin treatment before harvesting the fibroblasts. For this, fibroblasts of patient H.4 and two unrelated healthy controls were treated with bradykinin for either 0 min, 30 min or 60 minutes.

In normal fibroblasts bradykinin stimulates the release of IP3 which leads to IP3R3 activation and subsequent degradation of activated receptor via the UPP. Figure 10 demonstrates that IP3R3 degradation upon stimulation was completely abolished in patient fibroblasts, whilst control cell lines showed a stable decrease of IP3R3 levels to ~ 20 % - 60 % of baseline levels 60 min after bradykinin treatment.

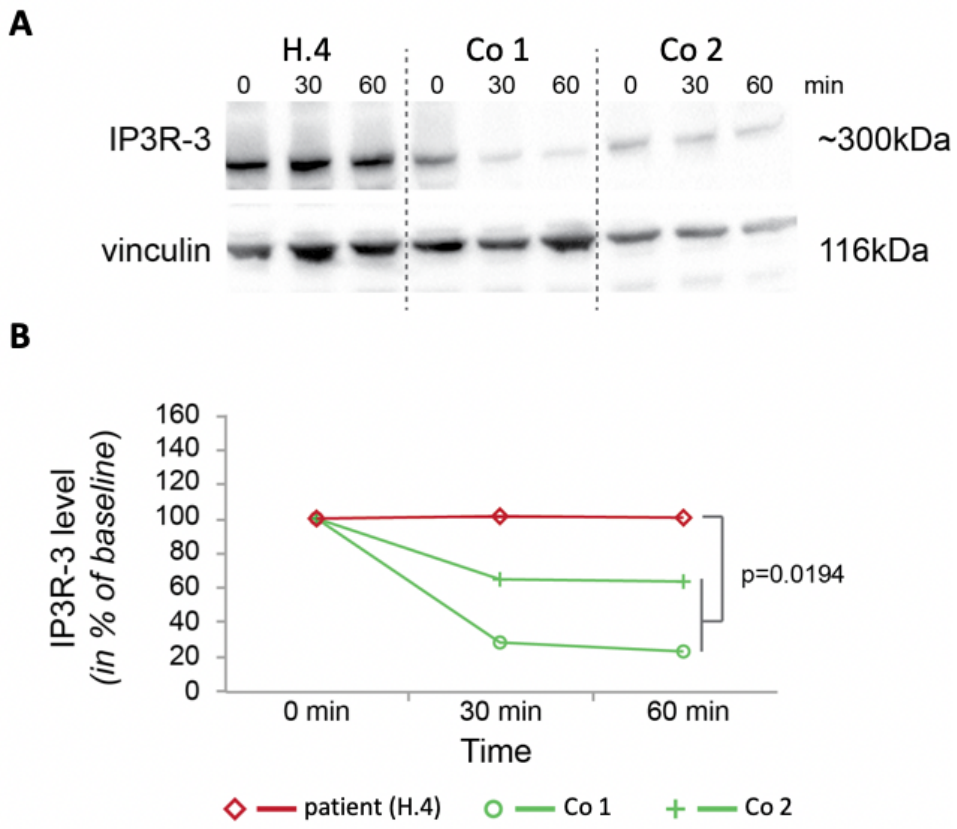

Figure 10: Accumulation of IP3R3 in patient H.4 fibroblasts upon bradykinin treatment. ***(A)*** *Western Blot analysis of patient H.4 fibroblasts and two control cell lines at baseline and after treatment with bradykinin for 30min and 60min. Loss of RNF170 results in abolished degradation of IP3R3 upon bradykinin stimulation in patient fibroblasts whilst control lines show a physiological decrease of IP3R3 levels upon stimulation. Western blots from a representative experiment are shown. Vinculin was used as a loading control.* ***(B)*** *Line diagram shows IP3R3 expression levels in % of baseline. Both control cell lines show a physiological decrease in IP3R3 levels, whilst levels where stable in patient cells (repeated measures ANOVA). Each data point represent means of three technical replicates (n=3). Modified from* (Wagner *et al.*, 2019).

4. Discussion

Hereditary spastic paraplegias are a genetically extremely heterogenous group of monogenic neurodegenerative diseases (Klebe, Stevanin and Depienne, 2015). Although a multitude of disease causing genes are already known, about one third of all cases still remains without molecular diagnosis (Schüle *et al.*, 2016). In this study we performed a step wise analysis approach on NGS data of two siblings with yet unsolved HSP. After genetic filtering via the GENESIS pipeline (Gonzalez *et al.*, 2015) we identified five candidate genes and were able to reduce them down to only one remaining candidate via segregation analysis across the family. As the remaining variant (*RNF170*) is located intronically and was predicted to affect splicing (Berkeley Drosophila Genome Project (REESE *et al.*, 1997)), we confirmed the pathogenicity of the variant via RNA studies. These demonstrated that the mutation affects splicing, resulting in an aberrant transcript lacking exon 5. The splice defects lead to a shift of the reading frame which is predicted to cause a premature stop codon leading to absent or a truncated (and probably dysfunctional) protein. In order to confirm this predicted effect we performed qRT-PCR with mRNA derived from patient fibroblasts and peripheral blood cells as well as RNF170 western blotting. Thereby we could demonstrate significantly reduced RNF170 mRNA expression levels (50%/36% of normal mRNA in fibroblasts/peripheral blood cells). Western blot analysis showed no residual RNF170 protein expression in patient fibroblasts.

Parallel to this expression experiments we performed a web search via GeneMatcher collaboration platform (Sobreira *et al.*, 2015) and were able to identify three additional families with seven additional individuals suffering from HSP whilst carrying biallelic loss of function (LOF) mutations in RNF170. Identification of these additional families is a crucial step to prove the causal relationship between RNF170 variants and the HSP phenotype, as a mutation in one single family - even if a functional effect of the variant can be demonstrated - is not sufficient to clinically and genetically prove the causality of this variant for the phenotype.

To gain further evidence for the cellular mechanism of RNF170 deficiency in mutated cells we performed western blots for IP3R3 in patient fibroblasts. As RNF170 operates as an ubiquitin ligase, which marks IP3R´s via ubiquitination for degradation, we showed that loss of RNF170 results in increased basal IP3R3 (main isoform in fibroblasts) levels in patient cells and thus affects basal turnover of IP3R3s. To additionally evaluate the effect of RNF170 deficiency on IP3R3 degradation upon activation we stimulated receptor degradation in fibroblasts via bradykinin-treatment and demonstrated that degradation was completely abolished in patient cells.

4.1 Relevance of NGS technologies and global matchmaking in solving families with rare Mendelian diseases

The evaluation of NGS datasets and subsequent validation via segregation analysis as well as consecutive genetic matchmaking can be used to contribute to the discovery of new disease genes and thereby expand the greater understanding of the pathophysiological mechanisms underlying rare Mendelian diseases in general.

Numerous other examples of this successful approach, also used in the present work, exist in the literature; only a few of them are mentioned in the following section. For example Wang et al. identified via WES a novel causative gene for spinocerebellar ataxias (*TGM6*) in two unrelated families (Wang *et al.*, 2010), Norton and colleagues used NGS to identify *BAG3* as a new causative gene for familial dilated cardiomyopathy in five unrelated families (Norton *et al.*, 2011) and Becker et al. did the same for identification of truncating mutations in *SERPINF1* in three families suffering from autosomal recessive osteogenesis imperfecta (Becker *et al.*, 2011).

In this early period of NGS related gene discoveries in rare monogenic diseases matchmaking was predominantly performed over patient cohorts from single clinical laboratories or by collaboration with peer group researches who already used to know each other personally.

Especially when it comes to very rare diseases with just a few affected patients all over the world this strategy becomes rather inefficient, which is why it

partially changed, with the emerging of global matchmaking tools like Gene matcher (Sobreira *et al.*, 2015). Using this global matchmaking tools Au et al. identified a novel malformation syndrome with symptoms like intellectual disability and characteristic facial dysmorphisms caused by de novo mutations in *HNRNPK* (Au *et al.*, 2015), Assoum and colleagues identified *AP3B2* as genetic cause for autosomal recessive epileptic encephalopathy with optic atrophy (Assoum *et al.*, 2016), and there are numerous other examples in the literature, which would far exceed the scope of this thesis.

All these examples demonstrate that the now widespread use of NGS technologies, especially in combination with effective global networking capabilities such as Gene Matcher, represents an immense advance in terms of new gene discoveries and thereby finding a molecular genetic diagnosis especially for families suffering from (ultra) rare diseases.

Nevertheless this approach also has some limitations. On the one hand, the correct analysis of NGS data involves some bioinformatic challenges. If sufficient quality control of the sequencing data, alignment and variant calling is not ensured, this may result in false candidate variants that cannot be confirmed via segregation analysis and thus represent an inefficient research approach. Second, the right interpretation of the numerous genetic variants identified by NGS is a major challenge. It is known that one single exome results in approximately 20.000 single nucleotide variants, indeed the vast majority of these are not deleterious (Frebourg, 2014). Among these, the so-called variants of unknown significance (VUS) represent a large group of potentially deleterious variants that would require extensive functional assessment which is beyond the opportunities of many studies.

Also regarding global matchmaking, there are some limitations. First, these matchmaking tools are usually freely available and each submitter thus decides which genes to upload as candidates. Thereby, the actual success of a match depends largely on the individual accuracy with which the submitted candidate genes have been internally validated. In addition, a single submitter may incur a high effort due to manual communication with the respective matched colleagues in case of numerous candidates, which could possibly slow down

the process, and depending on different clinical standards in phenotype description and diagnostics, initially assumed matches may in fact turn out to represent different diseases.

Last but not least, Hamosh et al. showed that five of the 20 most populous countries in the world do not yet have a single entry in GeneMatcher (Hamosh *et al.*, 2022), although this is one of the most widely used matchmaking platforms. This results in a population bias, presumably due to socioeconomic challenges, and obviously represents a significant limitation to the discovery of additional rare disease genes.

4.2 Relevance of non-coding variants for gene discovery in rare Mendelian disorders

In the beginning of gene discoveries via NGS data the main focus was on pathogenic coding variants, since widely used WGS was not affordable and in silico prediction tools for non-coding variants were just in the beginning. However, since WGS has mostly become a part of routine diagnostics and thanks to improved prediction tools, it is now possible to identify and confirm non-coding and regulatory variants more easily, in order to genetically solve some families with rare Mendelian disorders. For example in our index family WGS data analysis combined with in silico splice prediction revealed that the *RNF170* variant might have effects on splicing. Via cDNA analysis we were able to confirm this predicted effect, as the respective mutation leads to a loss of exon 5 during splicing, which presumably results in a shift of the reading frame. Western blot analysis showed no residual truncated protein which could be a consequence of either NMD or due to instability of a possible truncated protein. Even in case of expression of a truncated protein this would lack parts of the RING domain, which holds the E3 ligase activity, and therefore most likely be dysfunctional (Shenoy, 2016, pp. 148 - 149). A loss of function mechanism of RNF170 can therefore be assumed for the disease.

The relevance of this non-coding variants in disease gene identification both in HSP and other neurodegenerative diseases, e.g. ataxia, is underlined by various works already published. For example leads a homozygous intronic

splice site mutation in *SERAC1* gene to loss of the full-length protein and causes cHSP (Roeben *et al.*, 2018). Another study found a deep-intronic autosomal-recessive mutation in *POLR3A* (c.1909 +22G4A) as frequent cause of hereditary spastic ataxia, which was predicted to activate a cryptic splice site which could be confirmed via cDNA analysis. Furthermore, particularly interesting in this work, patients with intronic *POLR3A* variants showed a quite different phenotype from the so far known *POLR3A*-related syndromes highlighting a possible relevance of deep-intronic variants on disease aetiology (Minnerop *et al.*, 2017).

In summary, all these data highlight the increasing relevance of non-coding regions for the identification of novel disease genes in order to find a genetic diagnosis for rare Mendelian disorders.

4.3 Phenotypic characteristics of known mutations in *RNF170* and possible genotype-phenotype correlations

Up to date, there are two distinct phenotypes known to be caused by mutations in *RNF170*. On the one hand, the autosomal recessive HSP, which we first described (Wagner *et al.*, 2019), amongst others according to the data generated in this work, on the other hand the previously reported autosomal dominant sensory ataxia (ADSA) caused by a c.595C>T (p.Arg199Cys) missense mutation in *RNF170* (Valdmanis *et al.*, 2011).

As described in the results (3.2.3), all affected HSP patients with biallelic mutations in *RNF170* present with an early onset (2 to 5 years), slowly progressive spastic paraplegia, often accompanied by optic atrophy (7 of 9 patients) and cerebellar ataxia (6 of 9 patients). Meanwhile, in addition to the four families we described, three additional families with this new form of autosomal recessive HSP could be identified, which contributes to a broadening of the phenotypic spectrum of this newly discovered disease gene and opens new insights regarding genotype-phenotype correlations.

In a consanguineous family with roots in Guinea, a homozygous c.342C > G; p.(Tyr114*) stop gain variant in *RNF170* was found in all four affected siblings. The phenotypes of the patients predominantly corresponded to those already

described by us representing with infancy onset HSP, except for the optic atrophy, however this elaborate investigation was not performed in the mostly underage patients (Sainte Agathe *et al.*, 2021).

In addition, the authors hypothesize that the cerebellar symptoms seen in some patients may occur due to a toxic gain of function of aberrant mRNA, as they are predominantly seen in patients with variants known to generate transcripts which - at least partially - escape nonsense mediated decay (NMD) (Sainte Agathe *et al.*, 2021). This interesting theory could be further investigated by testing the additionally discovered *RNF170* variants in the following families for the ability to escape NMD.

Next, Chouery et al. found a missense variant in *RNF170* (NM_030954.3; p.Cys107Trp) in a 7-year-old Iraqi girl of consanguineous origin, which was identified as likely pathogenic according to the ACMG guidelines and predicted to affect splicing. Unfortunately, no RNA could be obtained from the patient, so the actual relevance of this variant could not be confirmed with certainty. Clinically, however, the symptoms are very consistent with those already described, but an examination for optic atrophy was not performed. With a mild intention tremor of the hands, there is evidence for cerebellar involvement in the patient (Chouery, Mehawej and Megarbane, 2022).

Most recently, another *RNF170* variant was found in a consanguineous Chinese family with HSP (Fu *et al.*, 2023). The particularly interesting fact about this patient, in whom the authors could identify a homozygous c.190C>T (p.R64*) mutation in *RNF170* (NM_030954.3) as disease-causing, was the comparatively late age at onset (15 years). From this age, the patient suffered lower limb spasticity with gait disturbance and a slightly ataxic gait pattern. Besides, MRI showed a mild cerebellar atrophy, an optic atrophy was not present. Apart from the significantly later onset of the disease, these symptoms are largely compatible with the phenotype described so far. In search of an explanation for the milder phenotype in this patient (represented by the older age at onset), the authors hypothesized that it might be due to the relatively upstream localization of the c.190C>T (p.R64*) variant compared to the other known variants. This could be relevant, as one isoform of the naturally occurring

mRNA transcripts for *RNF170* (transcript Q96K19-6), should theoretically be unaffected by this mutation, as it is located in the untranslated region (UTR) of this transcript. Therefore, a possible rescue effect of this transcript in the patient was speculated. However, quantitative RNA analysis of peripheral blood cells showed, that the mRNA levels of this transcript were significantly reduced in the patient, as well as levels of the dominant isoform (Q96K19-1) which confirmed the loss of function hypothesis for this variant (Fu *et al.*, 2023).
However, since RNA analyses were only performed on peripheral blood cells of the adult patient, it is possible that in other tissues, e.g. neuronal cells, or at an earlier developmental stage, other expression patterns for the transcripts existed, which could be accountable for a possible rescue effect. To further investigate the relevance of this particular transcript (Q96K19-6), further studies e.g. in zebrafish or iPSC derived cortical neurons are needed. Additionally RNA analysis for this particular transcript in some of the other RNF170 patients would be helpful (Fu *et al.*, 2023).

In contrast to RNF170-HSP, where multiple pathogenic mutations are known to be disease causing in all families, the same dominant missense variant in RNF170 is responsible for all ADSA cases known to date. Initially, a common founder effect was assumed, as the mutation was first discovered in two Canadian families (Valdmanis *et al.*, 2011). In the meantime, however, two additional families from different ethnic inheritance have been identified in which the exact same mutation occurs in combination with the respective clinic described for an ADSA (Cortese *et al.*, 2020; Van Daele *et al.*, 2022).
In this disorder, sensory ataxia occurs at older ages (4th-8th decade) due to length-dependent impairment of the central sensory tract (Valdmanis *et al.*, 2011; Cortese *et al.*, 2020; Van Daele *et al.*, 2022). In the Ecuadorian family, the phenotypic spectrum of the p.Arg199Cys variant could be extended, because an involvement of the sensory peripheral nerves as well as a bilateral vestibular areflexia was observed (Cortese *et al.*, 2020).

Starting with the different modes of inheritance, but also regarding the respective phenotype, there are few similarities between RNF170-HSP and RNF170-ADSA, which is why two different disease-causing pathomechanisms are assumed. This is also reflected at the molecular level; even though in both RNF170-HSP and RNF170-ADSA the mutations lead to reduced protein expression, in HSP this is caused by reduced expression of mutant RNF170, whereas in ADSA the mutation reduces RNF170 levels via increased auto-ubiquitination followed by degradation of the mutant protein. Since we have not detected a truncated protein in our RNF170-HSP index patient, a pure LOF mechanism is likely in this case. In the case of ADSA, however, the residual expression of a mutated protein could additionally lead to a toxic gain of function with resulting damage to the long sensory pathways. In contrast, the pyramidal system appears to be spared in ADSA - possibly due to the higher residual RNF170 activity of the wild-type allele (Wright *et al.*, 2015; Wagner *et al.*, 2019). Furthermore there are also differences regarding IP3R signaling, which will be discussed in more detail in the following section.

Overall, the increasing number of patients known to be affected by RNF170 associated disease highlights the potential clinical and diagnostic relevance of this new subtype of autosomal recessive HSP, even amongst rare diseases. With increasing numbers of affected patients, the need of possible future targeted therapies increases as well and thereby also becomes more promising. Nevertheless, it will be necessary to identify further cases in order to allow a broader understanding of genotype-phenotype correlations in the future.

4.4 Possible relevance of RNF170 deficiency on IP3R signaling and Ca^{2+} metabolism in HSP

As shown in Figure 9 (3.3.1) we could demonstrate that basal IP3R3 levels were increased approximately 4-fold in patient H.4´s fibroblasts compared to four unrelated healthy control cell lines which supports the hypothesis, that loss of RNF170 results in reduced ubiquitination and proteasomal degradation of IP3R3, causing an accumulation of IP3R3 in patient cells. To additionally investigate the RNF170 ligase effects under stimulated conditions a bradykinin

treatment was performed. Thereby we were able to show that IP3R3 degradation upon stimulation was completely abolished in patient fibroblasts, whilst control cell lines showed a physiological, stable decrease of IP3R3 levels to ~ 20 % - 60 % of baseline levels 60 min after treatment (Figure 10, 3.3.2).

Our data confirms the hypothesis that mutant RNF170 lacks the capability to ubiquitylate IP3R´s under both basal and stimulated conditions in fibroblasts.

While working on our publication (Wagner *et al.*, 2019), other members of the lab were able to replicate the results obtained in family HIH19851 in fibroblasts from another RNF170 family (Family 3, female patient) and thereby strengthen the evidence. Moreover, they were able to demonstrate that even in a neuronal model of RNF170 deficiency, obtained through CRISPR/Cas9 knockout of RNF170 in SH-SY5Y cells, IP3R1 levels were increased 1.8-fold compared to wildtype SH-SY5Y cells and this accumulation could be rescued by re-expression of wildtype RNF170 (Wagner *et al.*, 2019). This is particularly interesting, because IP3R1 represents the predominant receptor isoform in neuronal cells. The impairment of both basal and stimulus-dependent turnover of IP3R we observed in patient fibroblasts could thus also be confirmed in neurons.

Our results also fit with insights that other researchers had found in previous studies. For example *in vitro* studies investigating the IP3R1 levels in gonadotrophic αT3-1 pituitary mouse cells after CRISPR/Cas9 knockout of RNF170 showed increased IP3R1 levels under both basal and stimulated conditions (Wright *et al.*, 2015). Furthermore, Kim et al. generated RNF170 knockout mice, which even showed age-dependent progressive gait abnormalities that are consistent with the phenotype of human HSP and demonstrated *in vivo* that IP3R1 protein levels were elevated in spinal cord and cerebellum of these knockout mice (Kim *et al.*, 2015).

In contrast, gonadotrophic αT3-1 pituitary mouse cells containing the ADSA R199C variant demonstrate an intact RNF170 E3 ligase activity with normal IP3R1 levels indicating that ubiquitination of IP3R1 is not impaired in ADSA. Moreover, intracellular Ca^{2+} mobilization via IP3R is even decreased in patient lymphoblasts, but the distinct mechanism leading to this decrease remains

unclear (Wright *et al.*, 2015; Wagner *et al.*, 2019). Overall, in contrast to RNF170-HSP, a toxic gain of function is assumed as the underlying pathomechanism in RNF170-ADSA, a hypothesis which is also supported by Valdmanis et al.´s zebrafish studies (Valdmanis *et al.*, 2011).

Based on this cumulative evidence that loss of RNF170 increases IP3R levels, it seems likely that RNF170 deficiency leads to increased IP3R signaling, which could result in increased and prolonged Ca^{2+} efflux from the ER and in turn effect multiple cellular regulatory processes especially in neurons. This hypothesized effect on calcium metabolism as well as the actual effect on IP3R1 levels in neuronal cells of RNF170-HSP patients remains uncertain and requires further investigations.

4.5 Possible relevance of IP3R signaling as a candidate key pathway for future targeted therapies in HSP and neurodegenerative diseases

As already mentioned in the introduction (Figure 3) there are several additional players involved in IP3R-dependent Ca^{2+} signaling with lots of known mutations to cause neurodegenerative diseases which makes our finding of RN170-HSP even more interesting.

Firstly, several mutations of the receptor itself have been identified to cause spinocerebellar ataxia (SCA) and Gillespie syndrome. Genomic deletions of IP3R1 are causative for autosomal dominant adult onset slowly progressive cerebellar ataxia classified as SCA15. Secondly, autosomal dominant SCA29, a congenital infancy onset ataxia with hypotonia and mild cognitive impairment, has been shown to be caused by missense mutations in IP3R1. Thirdly, Gillespie syndrome, a rare neurological disease with iris hypoplasia, congenital ataxia, hypotonia and cognitive impairment has been associated with heterozygous dominant and biallelic recessive mutations in IP3R1 (Wagner *et al.*, 2019). Interestingly, in vitro analyses showed that these genomic deletions of IP3R1 and some of the missense mutations impaired receptor function after stimulation (Uchida *et al.*, 2003; Synofzik *et al.*, 2018) e.g. via insufficient IP3

binding or by inhibiting necessary conformational changes for channel opening (Ando, Hirose and Mikoshiba, 2018) which resulted in an aberrant, reduced Ca^{2+} release from the ER (Wagner *et al.*, 2019). The same could also be shown *in vivo* for *opisthotonos* mice which originated spontaneously from a laboratory mice colony and demonstrated a deletion of two exons of the IP3R1 gene together with an ataxic phenotype (Street *et al.*, 1997; Wagner *et al.*, 2019).

The next important key player in degradation of IP3Rs besides RNF170 is the ERLIN1/ERLIN2 complex. Variants in both of these genes are known to cause neurodegenerative diseases like HSP, amyotrophic lateral sclerosis (ALS) and primary lateral sclerosis (PLS). In particular, several ERLIN1 mutations (truncating and missense variants) have been shown to cause autosomal recessive early-onset complicated HSP (SPG62) (Novarino *et al.*, 2014) as well as juvenile ALS (Tunca *et al.*, 2018; Wagner *et al.*, 2019). On the other hand, autosomal recessive truncating ERLIN2 mutations are also known to manifest as childhood-onset complicated HSP (SPG18) (Alazami *et al.*, 2011; Yıldırım *et al.*, 2011; Wakil *et al.*, 2013) or PLS (Al-Saif, Bohlega and Al-Mohanna, 2012; Wagner *et al.*, 2019). Moreover, it has been recently shown that missense mutations in ERLIN2 can also cause autosomal dominant pure HSP and up to date there are four known missense mutations (p.S129T, p.T65I, p.V168M, p.A151V) in more than 5 families with partially very large pedigrees (Rydning *et al.*, 2018; Wright *et al.*, 2018; Amador *et al.*, 2019; Park *et al.*, 2020; Chen *et al.*, 2021). In some of the cases (two families), HSP converted into rapidly progressive ALS about more than two decades after HSP diagnosis, which is especially relevant regarding genetic counseling of families carrying ERLIN2 variants (Amador *et al.*, 2019). Most recently, two ERLIN2 missense variants have been associated with sporadic pure HSP, demonstrating that ERLIN2-associated disease and inheritance pattern is far more complex than initially assumed (Amador *et al.*, 2019; Srivastava *et al.*, 2020). These new findings increase the number of disease-causing mutations involved in the IP3R degradation, which reinforces the pathological relevance of this pathway in neurodegenerative diseases.

Even more interesting is the fact that the further experiments which were conducted in order to investigate the functional relevance of pathogenic mutations in the ERLIN1/2 genes matched to our findings for patient fibroblasts carrying mutant RNF170 (Wagner *et al.*, 2019). ERLIN1 as well as ERLIN2 knockout have been demonstrated independently to increase basal IP3R1 levels in gonadotrophic αT3-1 pituitary mouse cells and lead to an abolished stimulation dependent IP3R1 degradation as well. Furthermore, these effects were also found in pituitary mouse cells expressing one of the pathogenic ERLIN2 missense variants (p.T65I) (Wright *et al.*, 2018; Wagner *et al.*, 2019).

In summary, the data discussed in this section suggest that most pathogenic mutations in either ERLIN1, ERLIN2 or RNF170, with the exception of the RNF170-ADSA variant (Wright *et al.*, 2015), affect their coordinated action in the degradation of IP3Rs and thereby lead to increased IP3R levels due to impaired receptor degradation. If the elevated IP3R level in fact leads to increased intracellular Ca^{2+} signaling, like hypothesized before, has yet to be demonstrated, but would be a unifying characteristic of all mutations presenting with an HSP phenotype (Wagner *et al.*, 2019). On the other hand, reduced Ca^{2+} release from the ER seems to be more common in ataxic phenotypes, as it has been associated with several IP3R1 mutations in SCAs and Gillespie syndrome (Ando, Hirose and Mikoshiba, 2018; Wagner *et al.*, 2019).

Especially against the background that dysregulated IP3R-dependent Ca^{2+} signaling has already been linked to several other neurodegenerative diseases, inter alia SCA2 (Kasumu *et al.*, 2012), SCA3 (Chen *et al.*, 2008), Huntington's disease (Tang *et al.*, 2003), Parkinson's disease (Pchitskaya, Popugaeva and Bezprozvanny, 2018) and Alzheimer's disease (Tong *et al.*, 2018), this signaling pathway appears to be particularly promising for therapeutic research (Wagner *et al.*, 2019). Considering this data altogether, IP3R-dependent Ca^{2+} signaling evolves as a candidate key pathway for future targeted therapies not only in HSPs but also in other more common neurodegenerative diseases.

4.6 Conclusion and Outlook

This study was designed in order to solve undiagnosed families suffering from rare forms of HSP via identifying new disease genes. With identification of *RNF170* gene as causative for autosomal recessive HSP we were able to end the diagnostic odyssey for at least nine affected individuals from four families. Furthermore, in the last 3.5 years since our publication, three additional families have been identified (Sainte Agathe *et al.*, 2021; Chouery, Mehawej and Megarbane, 2022; Fu *et al.*, 2023), underlining the relevance of this particular new HSP gene. Considering the numerous disease-causing mutations in *RNF170* that have been identified so far, it should be pondered to add this gene to the established panels for HSPs and ataxias to increase their diagnostic value.

By further investigating the functional impact of pathogenetic RNF170 mutations in patient fibroblasts, we were able to identify RNF170 deficiency as harmful to both basal and stimulated IP3R turnover, which makes this signaling pathway - already known to be involved in neurodegeneration - a strong candidate for future targeted therapies in HSP and other neurodegenerative diseases.

To evaluate the pathogenetic relevance of our findings further investigations are required. First, our experiments could be repeated in cells from some of the meanwhile identified additional patients to confirm our results in a larger cohort. Second, further examinations in human post-mitotic neuronal cells are required, which could be generated for example via use of iPSCs. Furthermore, it would be fruitful to use iPSC-derived neurons or a vertebrate animal model e. g. mouse model (RNF170 knockout mice) for potential drug screenings.

As our study has shown, new gene discoveries are able to add more and more detail to already known facts, leading to a broader understanding of the pathomechanisms underlying a disease and thereby gain a better insight into the several processes and pathways involved in axon degeneration. The recognition of this pathways, and especially elucidating the interplay of multiple interactors in a given pathway is essential to develop pathway oriented therapies for rare inherited diseases in the future.

5. Abstract

Hereditary spastic paraplegias are a clinically and genetically extremely heterogenous group of monogenic neurodegenerative diseases. Their most prominent symptom is a slowly progressing lower limb spasticity and weakness caused by length dependent axonopathy of the upper motor neurons. Clinical classification distinguishes between pure and complicated forms of HSP. The latter variably includes additional symptoms like optic atrophy, cognitive impairment, ataxia and peripheral neuropathy. Mutations in more than 80 genes are known to cause autosomal dominant, recessive, X-linked and mitochondrial forms of the disease. Nevertheless, about one third of HSP cases remain unexplained by mutations in these known genes.

In this study we aimed at the identification of novel genes causing HSP in order to solve undiagnosed families and improve our understanding of the functional networks leading to axon degeneration. Thus we used WGS and WES data from a cohort of 142 individuals suffering from HSP without a molecular diagnosis. We used the GENESIS platform to apply a stepwise variant filtering approach on these NGS datasets and consecutively performed segregation analysis of top-ranked candidate variants. This approach led to identification of a novel candidate disease gene (*RNF170*) in an autosomal recessive family with two affected siblings. To confirm the functional effect of the c.396+3A>G variant, which was predicted to affect splicing, we performed RNA studies on patient peripheral blood cells and fibroblasts which demonstrated an aberrant transcript lacking exon 5 resulting in absent or a truncated protein. Accordingly, qRT-PCR showed significantly reduced *RNF170* expression levels in both cell types and western blot in patient fibroblasts showed no residual RNF170 protein.

As RNF170 works as an E3 ubiquitin ligase which targets IP3Rs for proteasomal degradation we performed additional western blots for IP3R3 in patient fibroblasts to gain more functional evidence about the consequences of RNF170 deficiency. Thereby we could demonstrate that loss of RNF170 impairs both basal and stimulation-dependent turnover of IP3Rs in mutant fibroblasts,

resulting in significant IP3R accumulation and indicating a possible effect of RNF170 deficiency on IP3R-dependent Ca^{2+} signaling.

To provide additional genetic proof for the pathogenetic relevance of the newly discovered gene we performed genetic matchmaking via the GeneMatcher collaboration platform and identified three more families with seven affected patients carrying biallelic loss of function mutations in *RNF170*.

Due to the growing number of publications which associated HSP as well as ADSA with *RNF170* mutations, this gene should be included in diagnostic panels for both ataxia and HSP.

If the functional impact seen on IP3R signaling in fibroblasts effectively transfers to Ca^{2+} homeostasis as well has yet to be examined. Moreover, further functional experiments in a suitable neuronal cell model, for example patient-derived iPSCs which can be differentiated to post mitotic-neuronal cells, are required.

Taken together the growing number of neurodegenerative diseases in which dysregulation of IP3R-dependent ER calcium release play an essential role emphasize that IP3R-dependent Ca^{2+} signaling may be a promising pathway for future targeted therapies in HSP and other diseases.

6. Zusammenfassung

Hereditäre spastische Paraplegien sind eine klinisch und genetisch heterogene Gruppe von monogenen neurodegenerativen Erkrankungen. Ihr Hauptsymptom ist eine langsam fortschreitende Spastik und Schwäche der unteren Extremität, die durch eine längenabhängige Axonopathie des ersten Motorneurons verursacht wird. Bei der klinischen Einteilung wird zwischen der reinen Form und der komplizierten HSP unterschieden, die variable zusätzliche Symptome wie Optikusatrophie, kognitive Beeinträchtigung, Ataxie und periphere Neuropathie aufweist. Es ist bekannt, dass Mutationen in mehr als 80 Genen autosomal dominante, rezessive, X-chromosomale und mitochondriale Formen der Krankheit verursachen. Dennoch bleibt etwa ein Drittel der HSP-Fälle durch Mutationen in diesen bekannten Genen unerklärt.

In dieser Studie hatten wir das Ziel neue HSP Gene zu identifizieren, um einige noch ungelöste Familien aufzuklären und unser generelles Verständnis der funktionellen Netzwerke zu verbessern, die zu Axondegeneration führen. Zu diesem Zweck haben wir WGS- und WES- Daten aus einer Kohorte von 142 Patienten mit HSP ohne molekularer Diagnose verwendet. Mittels eines schrittweisen Auswertungsverfahren dieser NGS-Daten durch zunächst genetisches Filtern unter Verwendung der GENESIS-Plattform und anschließender Segregationsanalyse innerhalb der Familie konnten wir ein verbleibendes Kandidatengen (RNF170) für eine autosomal rezessive Familie mit zwei betroffenen Geschwistern identifizieren. Um die Pathogenität der c.396+3A>G Variante zu bestätigen, für die prognostiziert war, dass sie das Spleißen beeinträchtigt, führten wir RNA-Analysen an Patientenproben durch (periphere Blutzellen und Fibroblasten) und konnten ein aberrantes Transkript nachweisen. Bei diesem Transkript kam es zu einem Verlust von Exon 5, was zu einem abwesenden oder verkürzten Protein führte. Entsprechend zeigte die qRT-PCR eine signifikant reduzierte RNF170 - Expression in beiden Zelltypen, und im Western Blot der Patientenfibroblasten war kein RNF170-Protein mehr nachweisbar.

Da RNF170 als E3-Ubiquitin-Ligase fungiert, die IP3Rs für den proteasomalen Abbau markiert, führten wir zusätzlich Western Blots für IP3R3 in

Patientenfibroblasten durch, um weitere funktionelle Erkenntnisse über die Folgen des RNF170-Mangels zu generieren. Dabei konnten wir zeigen, dass der Verlust von RNF170 sowohl den basalen als auch den stimulationsabhängigen Abbau von IP3Rs in den mutierten Fibroblasten beeinträchtigt, was eine mögliche Auswirkung auf die IP3R-abhängige Ca2+-Signalübertragung wahrscheinlich macht.

Um weitere genetische Beweise für die pathogenetische Relevanz des neu entdeckten Gens zu erbringen, haben wir über die GeneMatcher-Kollaborationsplattform eine genbasierte Suche durchgeführt und drei weitere Familien mit sieben betroffenen Patienten identifiziert, die bi-allelische, Funktionsverlustmutationen in RNF170 aufweisen.

Aufgrund der zunehmenden Zahl von Veröffentlichungen, die HSP und ADSA mit RNF170-Mutationen in Verbindung bringen, sollte dieses Gen in die diagnostischen Panels für Ataxie und HSP aufgenommen werden.

Ob die funktionellen Effekte, die bei der IP3R-Signalübertragung in Fibroblasten beobachtet wurden, auch auf die Ca2+-Homöostase übertragbar sind, muss noch untersucht werden. Darüber hinaus sind weitere funktionelle Experimente in einem geeigneten neuronalen Zellmodell erforderlich, z. B. an von Patienten generierten pluripotenten Stammzellen, die zu postmitotischen neuronalen Zellen differenziert werden können.

Nimmt man die zunehmende Anzahl an neurodegenerativen Erkrankungen zusammen, bei denen eine Dysregulation der IP3R-abhängigen Kalziumfreisetzung aus dem ER eine wesentliche Rolle spielt, wird deutlich, dass die IP3R-abhängige Ca2+-Signalübertragung ein vielversprechender Weg für zukünftige zielgerichtete Therapien bei HSP und anderen Erkrankungen sein könnte.

7. References

Sainte Agathe, J. *et al.* (2021) 'RNF170-Related Hereditary Spastic Paraplegia: Confirmation by a Novel Mutation', *Movement Disorders*, 36(3), pp. 771–774. Available at: https://doi.org/10.1002/mds.28371.

Al-Saif, A., Bohlega, S. and Al-Mohanna, F. (2012) 'Loss of ERLIN2 function leads to juvenile primary lateral sclerosis', *Annals of Neurology*, 72(4), pp. 510–516. Available at: https://doi.org/10.1002/ana.23641.

Alazami, A.M. *et al.* (2011) 'A nullimorphic ERLIN2 mutation defines a complicated hereditary spastic paraplegia locus (SPG18).', *Neurogenetics*, 12(4), pp. 333–6. Available at: https://doi.org/10.1007/s10048-011-0291-8.

Amador, M.-D.-M. *et al.* (2019) 'Spastic paraplegia due to recessive or dominant mutations in ERLIN2 can convert to ALS.', *Neurology. Genetics*, 5(6), p. e374. Available at: https://doi.org/10.1212/NXG.0000000000000374.

Ando, H., Hirose, M. and Mikoshiba, K. (2018) 'Aberrant IP3 receptor activities revealed by comprehensive analysis of pathological mutations causing spinocerebellar ataxia 29.', *Proceedings of the National Academy of Sciences of the United States of America*, 115(48), pp. 12259–12264. Available at: https://doi.org/10.1073/pnas.1811129115.

Assoum, M. *et al.* (2016) 'Autosomal-Recessive Mutations in AP3B2, Adaptor-Related Protein Complex 3 Beta 2 Subunit, Cause an Early-Onset Epileptic Encephalopathy with Optic Atrophy', *American Journal of Human Genetics*, 99(6), p. 1368. Available at: https://doi.org/10.1016/J.AJHG.2016.10.009.

Au, P.Y.B. *et al.* (2015) 'GeneMatcher aids in the identification of a new malformation syndrome with intellectual disability, unique facial dysmorphisms, and skeletal and connective tissue abnormalities caused by de novo variants in HNRNPK.', *Human mutation*, 36(10), pp. 1009–1014. Available at: https://doi.org/10.1002/humu.22837.

Becker, J. *et al.* (2011) 'Exome Sequencing Identifies Truncating Mutations in Human SERPINF1 in Autosomal-Recessive Osteogenesis Imperfecta', *American Journal of Human Genetics*, 88(3), p. 362. Available at: https://doi.org/10.1016/J.AJHG.2011.01.015.

Biesecker, L.G. (2010) *Exome sequencing makes medical genomics a reality*, *Nature Genetics*. Available at: https://doi.org/10.1038/ng0110-13.

Blackstone, C. (2012) 'Cellular Pathways of Hereditary Spastic Paraplegia', *Annual Review of Neuroscience*, 35(1), pp. 25–47. Available at: https://doi.org/10.1146/annurev-neuro-062111-150400.

Bokkala, S. and Joseph, S.K. (1997) 'Angiotensin II-induced Down-regulation of Inositol Trisphosphate Receptors in WB Rat Liver Epithelial Cells', *Journal of Biological Chemistry*, 272(19), pp. 12454–12461. Available at: https://doi.org/10.1074/jbc.272.19.12454.

Braschinsky, M. *et al.* (2009) 'The prevalence of hereditary spastic paraplegia and the occurrence of SPG4 mutations in Estonia.', *Neuroepidemiology*, 32(2), pp. 89–93. Available at: https://doi.org/10.1159/000177033.

Chen, S. *et al.* (2021) 'More autosomal dominant SPG18 cases than recessive? The first AD-SPG18 pedigree in Chinese and literature review', *Brain and Behavior*, 11(12), p. e32395. Available at: https://doi.org/10.1002/brb3.2395.

Chen, X. *et al.* (2008) 'Deranged calcium signaling and neurodegeneration in spinocerebellar ataxia type 3.', *The Journal of neuroscience : the official journal of the Society for Neuroscience*, 28(48), pp. 12713–24. Available at: https://doi.org/10.1523/JNEUROSCI.3909-08.2008.

Chouery, E., Mehawej, C. and Megarbane, A. (2022) 'A novel homozygous variant in RNF170 causes hereditary spastic paraplegia: a case report and review of the literature', *neurogenetics*, 23(2), pp. 85–90. Available at: https://doi.org/10.1007/s10048-022-00685-6.

Cortese, A. *et al.* (2020) 'Mutation in RNF170 causes sensory ataxic neuropathy with vestibular areflexia: a CANVAS mimic.', *Journal of neurology, neurosurgery, and psychiatry*, 91(11), pp. 1237–1238. Available at: https://doi.org/10.1136/jnnp-2020-323719.

Van Daele, S.H. *et al.* (2022) '*RNF170* mutation causes autosomal dominant sensory ataxia with variable pyramidal involvement', *European Journal of Neurology*, 29(1), pp. 345–349. Available at: https://doi.org/10.1111/ene.15091.

van Dijk, E.L. *et al.* (2014) 'Ten years of next-generation sequencing technology', *Trends in Genetics*, 30(9), pp. 418–426. Available at:

https://doi.org/10.1016/J.TIG.2014.07.001.

Erichsen, A.K. *et al.* (2009) 'Prevalence of hereditary ataxia and spastic paraplegia in southeast Norway: a population-based study', *Brain*, 132(6), pp. 1577–1588. Available at: https://doi.org/10.1093/brain/awp056.

Fink, J.K. (2013) 'Hereditary spastic paraplegia: clinico-pathologic features and emerging molecular mechanisms.', *Acta neuropathologica*, 126(3), pp. 307–28. Available at: https://doi.org/10.1007/s00401-013-1115-8.

Foskett, J.K. *et al.* (2007) 'Inositol Trisphosphate Receptor Ca $^{2+}$ Release Channels', *Physiological Reviews*, 87(2), pp. 593–658. Available at: https://doi.org/10.1152/physrev.00035.2006.

Frebourg, T. (2014) 'The Challenge for the Next Generation of Medical Geneticists', *Human Mutation*, 35(8), pp. 909–911. Available at: https://doi.org/10.1002/humu.22592.

Fu, J. *et al.* (2023) 'Novel stop-gain RNF170 variation detected in a Chinese family with adolescent-onset hereditary spastic paraplegia', *Clinical Genetics*, 103(1), pp. 87–92. Available at: https://doi.org/10.1111/cge.14219.

Lo Giudice, T. *et al.* (2014) 'Hereditary spastic paraplegia: Clinical-genetic characteristics and evolving molecular mechanisms', *Experimental Neurology*, 261, pp. 518–539. Available at: https://doi.org/10.1016/J.EXPNEUROL.2014.06.011.

Gonzalez, M. *et al.* (2015) 'Innovative genomic collaboration using the GENESIS (GEM.app) platform', *Human mutation*, 36(10), pp. 950–6. Available at: https://doi.org/10.1002/humu.22836.

Gonzalez, M.A. *et al.* (2013) 'GEnomes Management Application (GEM.app): a new software tool for large-scale collaborative genome analysis.', *Human mutation*, 34(6), pp. 842–6. Available at: https://doi.org/10.1002/humu.22305.

Hamosh, A. *et al.* (2022) 'The impact of GeneMatcher on international data sharing and collaboration', *Human Mutation*, 43(6), pp. 668–673. Available at: https://doi.org/10.1002/humu.24350.

Harding, A.E. (1983) 'Classification of the hereditary ataxias and paraplegias.', *Lancet (London, England)*, 1(8334), pp. 1151–5. Available at: https://doi.org/10.1016/s0140-6736(83)92879-9.

Hauser, S. *et al.* (2016) 'Establishment of SPAST mutant induced pluripotent stem cells (iPSCs) from a hereditary spastic paraplegia (HSP) patient.', *Stem cell research*, 17(3), pp. 485–488. Available at: https://doi.org/10.1016/j.scr.2016.09.022.

Hedera, P. (2021) *Hereditary Spastic Paraplegia Overview*, *GeneReviews®*. University of Washington, Seattle. Available at: http://www.ncbi.nlm.nih.gov/pubmed/21620353 (Accessed: 22 December 2022).

Kasumu, A.W. *et al.* (2012) 'Chronic Suppression of Inositol 1,4,5-Triphosphate Receptor-Mediated Calcium Signaling in Cerebellar Purkinje Cells Alleviates Pathological Phenotype in Spinocerebellar Ataxia 2 Mice', *Journal of Neuroscience*, 32(37), pp. 12786–12796. Available at: https://doi.org/10.1523/JNEUROSCI.1643-12.2012.

Kenwrick, S. *et al.* (1986) 'Linkage studies of X-linked recessive spastic paraplegia using DNA probes.', *Human genetics*, 73(3), pp. 264–6. Available at: https://doi.org/10.1007/BF00401241.

Khan, M.T. and Joseph, S.K. (2003) 'Proteolysis of type I inositol 1,4,5-trisphosphate receptor in WB rat liver cells.', *The Biochemical journal*, 375(Pt 3), pp. 603–11. Available at: https://doi.org/10.1042/BJ20030828.

Kim, Y. *et al.* (2015) 'Age-dependent gait abnormalities in mice lacking the *Rnf170* gene linked to human autosomal-dominant sensory ataxia', *Human Molecular Genetics*, 24(25), pp. 7196–7206. Available at: https://doi.org/10.1093/hmg/ddv417.

Klebe, S., Stevanin, G. and Depienne, C. (2015) 'Clinical and genetic heterogeneity in hereditary spastic paraplegias: From SPG1 to SPG72 and still counting', *Revue Neurologique*, 171(6–7), pp. 505–530. Available at: https://doi.org/10.1016/j.neurol.2015.02.017.

Kovalevich, J. and Langford, D. (2013) 'Considerations for the use of SH-SY5Y neuroblastoma cells in Neurobiology.', *Methods in molecular biology (Clifton, N.J.)*, 1078, pp. 9–21. Available at: https://doi.org/10.1007/978-1-62703-640-5_2.

Liu, J. *et al.* (2009) 'Deranged calcium signaling and neurodegeneration in

spinocerebellar ataxia type 2', *The Journal of neuroscience : the official journal of the Society for Neuroscience*, 29(29), pp. 9148–62. Available at: https://doi.org/10.1523/JNEUROSCI.0660-09.2009.

Lu, J.P. *et al.* (2011) 'RNF170 protein, an endoplasmic reticulum membrane ubiquitin ligase, mediates inositol 1,4,5-trisphosphate receptor ubiquitination and degradation', *The Journal of biological chemistry*, 286(27), pp. 24426–33. Available at: https://doi.org/10.1074/jbc.M111.251983.

McAllister, B.S. *et al.* (1993) 'Bradykinin receptors and signal transduction pathways in human fibroblasts: integral role for extracellular calcium.', *Archives of biochemistry and biophysics*, 304(1), pp. 294–301. Available at: https://doi.org/10.1006/abbi.1993.1352.

Minnerop, M. *et al.* (2017) 'Hypomorphic mutations in POLR3A are a frequent cause of sporadic and recessive spastic ataxia.', *Brain : a journal of neurology*, 140(6), pp. 1561–1578. Available at: https://doi.org/10.1093/brain/awx095.

Ng, S.B. *et al.* (2010) 'Exome sequencing identifies the cause of a Mendelian disorder.', *Nature genetics*, 42(1), pp. 30–5. Available at: https://doi.org/10.1038/ng.499.

Norton, N. *et al.* (2011) 'Genome-wide studies of copy number variation and exome sequencing identify rare variants in BAG3 as a cause of dilated cardiomyopathy.', *American journal of human genetics*, 88(3), pp. 273–82. Available at: https://doi.org/10.1016/j.ajhg.2011.01.016.

Novarino, G. *et al.* (2014) 'Exome Sequencing Links Corticospinal Motor Neuron Disease to Common Neurodegenerative Disorders', *Science*, 343(6170), pp. 506–511. Available at: https://doi.org/10.1126/science.1247363.

Olzmann, J.A., Kopito, R.R. and Christianson, J.C. (2013) 'The mammalian endoplasmic reticulum-associated degradation system.', *Cold Spring Harbor perspectives in biology*, 5(9). Available at: https://doi.org/10.1101/cshperspect.a013185.

Park, J.-M. *et al.* (2020) 'An autosomal dominant ERLIN2 mutation leads to a pure HSP phenotype distinct from the autosomal recessive ERLIN2 mutations (SPG18).', *Scientific reports*, 10(1), p. 3295. Available at: https://doi.org/10.1038/s41598-020-60374-y.

Pchitskaya, E., Popugaeva, E. and Bezprozvanny, I. (2018) ‘Calcium signaling and molecular mechanisms underlying neurodegenerative diseases.’, *Cell calcium*, 70, pp. 87–94. Available at: https://doi.org/10.1016/j.ceca.2017.06.008.

REESE, M.G. *et al.* (1997) ‘Improved Splice Site Detection in Genie’, *Journal of Computational Biology*, 4(3), pp. 311–323. Available at: https://doi.org/10.1089/cmb.1997.4.311.

Roeben, B. *et al.* (2018) ‘SERAC1 deficiency causes complicated HSP: evidence from a novel splice mutation in a large family.’, *Journal of medical genetics*, 55(1), pp. 39–47. Available at: https://doi.org/10.1136/jmedgenet-2017-104622.

Ruano, L. *et al.* (2014) ‘The Global Epidemiology of Hereditary Ataxia and Spastic Paraplegia: A Systematic Review of Prevalence Studies’, *Neuroepidemiology*, 42(3), pp. 174–183. Available at: https://doi.org/10.1159/000358801.

Rydning, S.L. *et al.* (2018) ‘A novel heterozygous variant in *ERLIN2* causes autosomal dominant pure hereditary spastic paraplegia’, *European Journal of Neurology*, 25(7), pp. 943-e71. Available at: https://doi.org/10.1111/ene.13625.

Schüle, R. *et al.* (2006) ‘The Spastic Paraplegia Rating Scale (SPRS): a reliable and valid measure of disease severity.’, *Neurology*, 67(3), pp. 430–4. Available at: https://doi.org/10.1212/01.wnl.0000228242.53336.90.

Schüle, R. *et al.* (2016) ‘Hereditary spastic paraplegia: Clinicogenetic lessons from 608 patients’, *Annals of Neurology*, 79(4), pp. 646–658. Available at: https://doi.org/10.1002/ana.24611.

Schüle, R. and Schöls, L. (2011) ‘Genetics of hereditary spastic paraplegias.’, *Seminars in neurology*, 31(5), pp. 484–93. Available at: https://doi.org/10.1055/s-0031-1299787.

Shenoy, S.K. (2016) *Ubiquitination and Transmembrane Signaling.*, *Progress in Molecular Biology and Translational Science*. Academic Press.

Sobreira, N. *et al.* (2015) ‘GeneMatcher: A Matching Tool for Connecting Investigators with an Interest in the Same Gene’, *Human Mutation*, 36(10), pp. 928–930. Available at: https://doi.org/10.1002/humu.22844.

Srivastava, S. *et al.* (2020) ‘Expansion of the genetic landscape of ERLIN2-

related disorders.', *Annals of clinical and translational neurology*, 7(4), pp. 573–578. Available at: https://doi.org/10.1002/acn3.51007.

Street, V.A. *et al.* (1997) 'The Type 1 Inositol 1,4,5-Trisphosphate Receptor Gene Is Altered in the *opisthotonos* Mouse', *The Journal of Neuroscience*, 17(2), pp. 635–645. Available at: https://doi.org/10.1523/JNEUROSCI.17-02-00635.1997.

Synofzik, M. *et al.* (2018) 'De novo ITPR1 variants are a recurrent cause of early-onset ataxia, acting via loss of channel function', *European Journal of Human Genetics*, 26(11), pp. 1623–1634. Available at: https://doi.org/10.1038/s41431-018-0206-3.

Tang, T.-S. *et al.* (2003) 'Huntingtin and huntingtin-associated protein 1 influence neuronal calcium signaling mediated by inositol-(1,4,5) triphosphate receptor type 1', *Neuron*, 39(2), pp. 227–39. Available at: https://doi.org/10.1016/s0896-6273(03)00366-0.

Tong, B.C.-K. *et al.* (2018) 'Calcium signaling in Alzheimer's disease & therapies', *Biochimica et Biophysica Acta (BBA) - Molecular Cell Research*, 1865(11), pp. 1745–1760. Available at: https://doi.org/10.1016/J.BBAMCR.2018.07.018.

Tunca, C. *et al.* (2018) 'ERLIN1 mutations cause teenage-onset slowly progressive ALS in a large Turkish pedigree', *European Journal of Human Genetics*, 26(5), pp. 745–748. Available at: https://doi.org/10.1038/s41431-018-0107-5.

Uchida, K. *et al.* (2003) 'Critical Regions for Activation Gating of the Inositol 1,4,5-Trisphosphate Receptor', *Journal of Biological Chemistry*, 278(19), pp. 16551–16560. Available at: https://doi.org/10.1074/JBC.M300646200.

Valdmanis, P.N. *et al.* (2011) 'A mutation in the RNF170 gene causes autosomal dominant sensory ataxia', *Brain*, 134(2), pp. 602–607. Available at: https://doi.org/10.1093/brain/awq329.

Velinov, M. *et al.* (2012) 'Mutations in the gene DNAJC5 cause autosomal dominant Kufs disease in a proportion of cases: study of the Parry family and 8 other families.', *PloS one*, 7(1), p. e29729. Available at: https://doi.org/10.1371/journal.pone.0029729.

Wagner, M. *et al.* (2019) ‘Bi-allelic variants in RNF170 are associated with hereditary spastic paraplegia.’, *Nature communications*, 10(1), p. 4790. Available at: https://doi.org/10.1038/s41467-019-12620-9.

Wakil, S.M. *et al.* (2013) ‘A novel splice site mutation in ERLIN2 causes hereditary spastic paraplegia in a Saudi family’, *European Journal of Medical Genetics*, 56(1), pp. 43–45. Available at: https://doi.org/10.1016/J.EJMG.2012.10.003.

Wang, J.L. *et al.* (2010) ‘TGM6 identified as a novel causative gene of spinocerebellar ataxias using exome sequencing’, *Brain*, 133(12), pp. 3510–3518. Available at: https://doi.org/10.1093/brain/awq323.

Wojcikiewicz, R.J.H. *et al.* (2009) ‘When worlds collide: IP3 receptors and the ERAD pathway’, *Cell Calcium*, 46(3), pp. 147–153. Available at: https://doi.org/10.1016/J.CECA.2009.05.002.

Wright, F.A. *et al.* (2015) ‘A Point Mutation in the Ubiquitin Ligase RNF170 That Causes Autosomal Dominant Sensory Ataxia Destabilizes the Protein and Impairs Inositol 1,4,5-Trisphosphate Receptor-mediated Ca2+ Signaling.’, *The Journal of biological chemistry*, 290(22), pp. 13948–57. Available at: https://doi.org/10.1074/jbc.M115.655043.

Wright, F.A. *et al.* (2018) ‘The erlin2 T65I mutation inhibits erlin1/2 complex–mediated inositol 1,4,5-trisphosphate receptor ubiquitination and phosphatidylinositol 3-phosphate binding’, *Journal of Biological Chemistry*, 293(40), pp. 15706–15714. Available at: https://doi.org/10.1074/jbc.RA118.004547.

Yıldırım, Y. *et al.* (2011) ‘A frameshift mutation of ERLIN2 in recessive intellectual disability, motor dysfunction and multiple joint contractures’, *Human Molecular Genetics*, 20(10), pp. 1886–1892. Available at: https://doi.org/10.1093/hmg/ddr070.

8. Confirmation of the contribution to authorship

Erklärung zum Eigenanteil der Dissertationsschrift

Diese Arbeit wurde im Hertie Institut für klinische Hirnforschung unter Betreuung von Prof. Dr. Rebecca Schüle durchgeführt.
Die Konzeption der Studie erfolgte durch Prof. Dr. Rebecca Schüle.
Die Patientendaten wurden von Prof. Dr. Rebecca Schüle zur Verfügung gestellt. Ergänzende Untersuchungen der zusätzlich identifizierten Familien wurden von Kooperationspartnern durchgeführt (Dr. Matias Wagner, Dr. Yalda Jamshidi).
Sämtliche Versuche wurden (nach Einarbeitung durch Jennifer Reichbauer, Selina Reich, Ulrike Ulmer) von mir eigenständig durchgeführt.
Die statistische Auswertung erfolgte nach Anleitung durch Prof. Dr. Rebecca Schüle durch mich.
Ich versichere, das Manuskript selbstständig verfasst zu haben und keine weiteren als die von mir angegebenen Quellen verwendet zu haben.

Tübingen, den 10.11.2023

9. Publications

Parts of this dissertation have already been published in the following publication:

- Wagner, M. *et al.* (2019) 'Bi-allelic variants in RNF170 are associated with hereditary spastic paraplegia.', *Nature communications*, 10(1), p. 4790. Available at: https://doi.org/10.1038/s41467-019-12620-9.

10. Supplement

Table 20: List of genes used for variant screening in known disease associated genes (2.2.1)

Gene	Locus	Mode of Inheritance	Gene	Locus	Mode of Inheritance	Gene	Locus	Mode of Inheritance
SEPT9	SEPT9	AD	*APTX*	AOA1	AR	*BSCL2*	SPG17/HMN5A	AD
AARS	CMT2N	AD	*ARG1*		unknown	*BTD*	BTD	AR
ABCB7	ABCB7	XR	*ARHGEF10*	ARHGEF10	AD	*C10orf2*	C10orf2	AD
ABCD1	ABCD1	XR	*ARHGEF28*		unknown	*C12orf65*	SPG55	AR
ABHD12	ABHD12	AR	*ARL13B*	JBTS8	AR	*C19orf12*	SPG43	AR
ACO2	ACO2	AR	*ARL6IP1*	SPG61	AR	*C2orf64*	CYTc	AR
ACOX1	ACOX1	AR	*ARSA*	MLD	AR	*C5ORF42*	JBTS17	AR
ADAR	ADAR	AR/AD	*ARSI*	SPG66	AR	*C7orf10*	C7orf10	AR
ADCK3	SCAR9/COQ10D4	AR	*ARX*	PRTS	XR	*CA8*	CAMRQ3	AR
ADCY5		unknown	*ATCAY*	ATCAY	AR	*CACNA1A*	SCA6/EA2	AD
ADD3	ADD3	AR	*ATL1*	SPG3/HSN1D	AD/AR	*CACNA1G*		unknown
ADGRG1		unknown	*ATL3*	ASN1F	AD	*CACNB4*	EA5	AD
AFG3L2	SCA28	AD	*ATM*	ATM	AR	*CAMTA1*		unknown
AFG3L2	SPAX5	AR	*ATN1*		AD	*CAPN1*	CAPN1	AR
AGO2	AGO2	unknown	*ATP13A2*	CLN12	AR	*CAPNS2*	CAPNS2	AR
AGPS	AGPS	AR	*ATP1A3*		unknown	*CAPRIN1*		unknown
AGXT	AGXT	AR	*ATP2B2*		unknown	*CASK*	MICPCH	XD
AHI1	JBTS3	AR	*ATP2B3*	SCAX1	XR	*CAT*	CAT	AR
AIF	CMTX4	XR	*ATP2B4*	ATP2B4	AD	*CC2D2A*	JBTS9	AR

Gene	Locus	Mode of Inheritance	Gene	Locus	Mode of Inheritance	Gene	Locus	Mode of Inheritance
AIMP1	HLD3	AR	*ATP2B4*		unknown	*CCDC88C*	CCDC88C	AD
ALAS2	ALAS2	XR	*ATP6*	ATP6	MT	*CCT5*	CCT5	AR
ALDH18A1	SPG9	AD/AR	*ATP7A*	SMAX3	XR	*CEP290*	JBTS5	AR
ALDH3A2		unknown	*ATP7B*	ATP7B	AR	*CEP41*	JBTS15	AR
ALG6	CDG1C	AR	*ATP8A2*	CAMRQ4	AR	*CHCHD10*		unknown
ALS2	ALS2	AR	*ATR*	ATR	AR	*CHMP1A*	PCD8	AR
AMACR	AMACR	AR	*ATXN1*	SCA1	AD	*CHMP2B*		unknown
AMPD2	SPG63	AR	*ATXN10*	SCA10	AD	*CHP1*	CHP1	unknown
AMT	GCE	AR	*ATXN2*	SCA2	AD	*CHRM1*		unknown
ANG	ALS9	AD	*ATXN3*	SCA3	AD	*CLCN2*	CLCN2	AR
ANO10	SCAR10	AR	*ATXN7*	SCA7	AD	*CLN2*	CLN2	AR
AP4B1	SPG47	AR	*ATXN8*	SCA8	AD	*CLN3*	CLN3	AR
AP4E1	SPG51	AR	*ATXN8/ATXN8 OSVA*	SCA8	AD	*CLN5*	CLN5	AR
AP4M1	SPG50	AR	*AUH*	MGA1	AR	*CLN6*	CLN4A / CLN6	AR
AP4S1	SPG52	AR	*B4GALNT1*	SPG26	AR	*CLN8*	CLN8	AR
AP5B1		unknown	*B9D1*	B9D1	AR	*COQ2*	COQ10D1	AR
AP5M1		unknown	*BCS1L*	MC3DN1	AR	*COQ6*	COQ10D6	AR
AP5S1		unknown	*BEAN1*	SCA31	AD	*COQ9*	COQ10D5	AR
AP5Z1	SPG48	AR	*BICD2*	SMALED2	AD	*COX10*	CYTc	AR
APOB	APOB	AR	*BIVM*		unknown	*COX15*	CYTc	AR
COX20	CYTc	AR	*EEF2*	SCA26	AD	*FGGY*		unknown

Gene	Locus	Mode of Inheritance	Gene	Locus	Mode of Inheritance	Gene	Locus	Mode of Inheritance
COX6B1	CYTc	AR	*EGR2*	CMT1D, CMT4E	AD/AR	*FIG4*	CMT4J	AR
CP	CP	AR	*EIF2B1*	VWM	AR	*FLRT1*	SPG68	AR
CPT1C	CPT1C	AD	*EIF2B2*	VWM	AR	*FLVCR1*	FLVCR1	AR
CRAT	CRAT	AR	*EIF2B3*	VWM	AR	*FMR1*		unknown
CSF1R		unknown	*EIF2B4*	VWM	AR	*FOLR1*	FOLR1	AR
CSTB	EPM1A	AR	*EIF2B5*	VWM	AR	*FTL*	NBIA3	AR
CTDP1	CTDP1	AR	*ELOVL4*	ELOVL4	AR	*FUS*	ALS6	AR
CTSD	CLN10	AR	*ELOVL5*	ELOVL5	AD	*FXN*	FXN	AR
CTSF	CLN13	AR	*ELP3*		unknown	*GAD1*	CPSQ1	AR
CWF19L1	*CWF19L1*	AR	*ENTPD1*	SPG64	AR	*GALC*	GALC	AR
CYC1	MC3DN6	AR	*EPM2A*	EPM2A	AR	*GAN*	GAN	AR
CYP27A1	CYP27A1	AR	*ERBB4*		unknown	*GARS*	CMT2D/HMN5A	AD
CYP2U1	SPG56	AR	*ERCC2*	XPD	AR	*GART*		unknown
CYP7B1	SPG5	AR	*ERCC3*	XPB	AR	*GBA*	GBA	AR
DAO		unknown	*ERCC4*	XPF	AR	*GBA2*	SPG46	AR
DARS		unknown	*ERCC5*	XPG	AR	*GBE1*	GBE1	AR
DARS2	DARS2	AR	*ERCC6*	CSB	AR	*GCDH*	GCDH	AR
DCAF8	HMSN2	AD	*ERCC8*	CSA	AR	*GCH1*	DYT5	AD/AR
DCTN1	HMN7B	AD	*ERLIN1*	SPG62	AR	*GCLC*	GCLC	AR
DDB2	XPE	AR	*ERLIN2*	SPG18	AR	*GCSH*	GCE	AR
DDHD1	SPG28	AR	*ETFA*	MADD	AR	*GDAP1*	CMT2K	AD
DDHD2	SPG54	AR	*ETFB*	MADD	AR	*GDAP1*	CMT4A/CMTR1A	AR

Gene	Locus	Mode of Inheritance	Gene	Locus	Mode of Inheritance	Gene	Locus	Mode of Inheritance
DDX17	DDX17	unknown	*ETFDH*	MADD	AR	*GFAP*	GFAP	AD
DDX5	DDX5	unknown	*EWSR1*		unknown	*GJB1*	CMTX1	XD
DHTKD1	CMT2Q	AD	*EXOSC3*	PCH1B	AR	*GJB3*	GJB3	AD
DKC1	DKC1	AR	*FA2H*	SPG35	AR	*GJC2*	SPG44/HLD2	AR
DLAT	PDHDD	AR	*FAM126A*	HLD5	AR	*GLB1*	GLB1	AR
DLD	DLD	AR	*FAM134B*	HSAN2B	AR	*GLDC*	GCE	AR
DNAJA3	DNAJA3	AR	*FARS2*	FARS2	AR	*GLE1*		unknown
DNAJB2	DSMA5	AR	*FASTKD2*	CYTc	AR	*GLRX5*		AR
DNAJC19	MGA5	AR	*FAT2*		AR	*GLTP*	SPG36	AD
DNAJC3	DNAJC3	AR	*FBLN5*	HMSN1	AD	*GM2A*	GM2A	AR
DNAJC5	CLN4B	AR	*FBXO38*	HMN2D	AD	*GNB4*	CMTDIF	AD
DNM2	CMT2M/CMTDIB	AD	*FBXO41*	FBXO41	unknown	*GNPAT*	GNPAT	AR
DNMT1	HSN1E	AD	*FBXO7*	FBXO7	AR	*GOSR2*	EPM6	AR
DPP6		unknown	*FEM1C*	FEM1C	AR	*GPR56*	GPR56	AR
DST	HSAN6	AR	*FGD4*	CMT4H	AR	*GRID2*	GRID2	AR
DYNC1H1	CMT2O/SMALED1	AD	*FGF14*	SCA27	AD	*GRM1*	SCAR13	AR
GRN	CLN11	AR	*KANK1*	CPSQ2	AR	*MFSD8*	CLN7	AR
GSN		unknown	*KARS*	CMTR1B	AR	*MKS1*	MKS1	AR
GSS	GSS	AR	*KCNA1*	EA1	AD	*MKS3*	MKS3	AR
GTF2H5	TTD	AR	*KCNA2*	KCNA2	AD	*MLC1*	MLC1	AR
HARS	HARS	AD	*KCNC1*	KCNC1	AD	*MMADHC*		AR
HEPACAM	HEPACAM	AR	*KCNC3*	SCA13	AD	*MME*	MME	AR/AD

Gene	Locus	Mode of Inheritance	Gene	Locus	Mode of Inheritance	Gene	Locus	Mode of Inheritance
HERC1		unknown	*KCND3*	SCA19/SCA22	AD	*MORC2*		AD
HEXA	HEXA	AR	*KCNJ10*	KCNJ10	AR	*MPZ*	CMT1B/CMTDID/ CMT2I	AD
HEXB	HEXB	AR	*KCTD7*	CLN14, EPM3	AR	*MPZ*	CMT4E	AR
HFE		unknown	*KIAA0196*	SPG8	AD	*MRE11A*	ATLD	AR
HINT1	NMAN	AR	*KIAA0226*	SCAR	AR	*MSTO1*		unknown
HK1	CMT4G	AR	*KIF1A*	SPG30/HSN2C	AD	*MTHFR*	MTHF3	AR
HNRNPA1		unknown	*KIF1A*	SPG30/HSN2C	AR	*MTMR2*	CMT4B1	AR
HNRNPA2B1		unknown	*KIF1B*	CMT2A1	AD	*MTPAP*	SPAX4	AR
HNRNPD		unknown	*KIF1C*	SPG58/SPAX2	AR	*MTRR*		unknown
HNRNPF	HNRNPF	unknown	*KIF5A*	SPG10	AD	*MTTP*	MTTP	AR
HNRNPH1	HNRNPH1	unknown	*KIF5C*	KIF5C	AR	*MYH4*	MYH4	AR
HNRNPH2	HNRNPH2	unknown	*KIF7*	JBTS12	AR	*NDRG1*	CMT4D	AR
HNRNPH3	HNRNPH3	unknown	*KLC4*	KLC4	AR	*NDUFS7*		unknown
HPRT1	HPRT1	XR	*KLHL40*	KLHL40	AR	*NEFH*		unknown
HSD17B4	HSD17B4	AR	*KPNA3*	KPNA3	AD	*NEFL*	CMT1F/CMT2E	AD
HSD17B8	HSD17B8	AR	*L1CAM*	SPG1	XR	*NEK1*		unknown
HSPB1	CMT2F/HMN2B	AD	*L2HGDH*	L2HGDH	AR	*NEU1*	NEU1	AR
HSPB3	HMN2C	AD	*LIAS*	PDHLD	AR	*NGFB*	HSAN5	AR
HSPB8	CMT2L/HMN2A	AD	*LITAF*	CMT1C	AD	*NHLRC1*	EPM2B	AR
HSPD1	HLD4/SPG13	AR/AD	*LMNA*	CMT2B1	AR	*NIPA1*	SPG6	AD
HTRA1	HTRA1	AR	*LMNB1*	LMNB1	AD	*NKX2-1*		unknown

Gene	Locus	Mode of Inheritance	Gene	Locus	Mode of Inheritance	Gene	Locus	Mode of Inheritance
IBA57	IBA57	AR	*LMNB2*		unknown	*NKX6-2*		AR
IFIH1	IFIH1	AD	*LRPPRC*	CYTc	AR	*NOL3*		unknown
IFRD1	SMNA	AD	*LRSAM1*	CMT2P	AD/AR	*NONO*	NONO	unknown
IFT140		unknown	*LYST*	LYST	AR	*NOP56*	SCA36	AD
IGDCC3		unknown	*MAG*	MAG	AR	*NPC1*	NPC1	AR
IGHMBP2	HMN6	AR	*MAPT*		unknown	*NPC2*	NPC2	AR
IKBKAP	HSAN3	AR	*MARS*	SPG70	AR	*NPHP1*	JBTS4	AR
INF2	CMTDIE	AD	*MARS2*	SPAX3	AR	*NT5C2*	SPG65	AR
INPP5E	JBTS1	AR	*MATR3*	MATR3	AD	*NTRK1*	HSAN4	AR
ITM2B	ITM2B	AD	*MECP2*		unknown	*NUBPL*		unknown
ITPR1	SCA15/SCA29/(SCA16)	AD	*MED25*	CMT2B2	AR	*OFD1*	JBTS10	XR
ITPR2		unknown	*MFN2*	CMT2A2/HMSN6	AD	*OPA1*	OPA1	AD
OPA3	MGA3/ OPA3	AR/AD	*PMP22*	CMT1A/HNPP	AD	*RPGRIP1L*	JBTS7	AR
OPTN	ALS12	AD/AR	*PMPCA*		AR	*RRM2B*		unknown
OTUD4	OTUD4	AD	*PNKP*	AOA4	AR	*RTN2*	SPG12	AD
PABPC1	PABPC1	unknown	*PNP*	PNP	unknown	*SACS*	SPAX6	AR
PANK2	NBIA1	AR	*PNPLA6*	SPG39	AR	*SBF1*	CMT4B3	AR
PARK7		unknown	*POLG*	POLG	AD/AR	*SBF2*	CMT4B2	AR
PAX6	PAX6	AR	*POLH*	XPV	AR	*SCN11A*	HSAN7	AD
PCNA		AR	*POLR3A*	HLD7	AR	*SCN8A*	SCN8A	AD
PDHA1	PDHA1	XD	*POLR3B*	HDL8	AR	*SCN9A*	SCN9A	AD

Gene	Locus	Mode of Inheritance	Gene	Locus	Mode of Inheritance	Gene	Locus	Mode of Inheritance
PDHB	PDHBD	AR	*PON1*		unknown	*SCO1*	CYTc	AR
PDHX	PDHXD	AR	*PON2*		unknown	*SCYL1*	SCYL1	AR
PDK3	CMTX6	X	*PON3*		unknown	*SDHA*	SDHA	AR
PDP1	PDHPD	AR	*PPP2R2B*	SCA12	AD	*SDHAF1*	SDHAF1	AR
PDSS1	COQ10D2	AR	*PPT1*	CLN1	AR	*SEC16A*		unknown
PDSS2	COQ10D3	AR	*PQBP1*	PQBP1	XR	*SEPSECS*	PCH2D	AR
PDYN	SCA23	AD	*PRICKLE1*	EPM1B	AR	*SERAC1*		unknown
PEX1	PDB1A	AR	*PRKCG*	SCA14	AD	*SETX*	ALS4/SCAR1/SCAN2	AD/AR/AR
PEX10	PDB6A	AR	*PRNP*	PRNP	AD	*SFPQ*	SFPQ	unknown
PEX12	PDB3A	AR	*PRPH*		unknown	*SH3TC2*	CMT4C/ MNMN	AR/AD
PEX13	PDB11A	AR	*PRPS1*	CMTX5	XR	*SIGMAR1*		unknown
PEX14	PDB13A	AR	*PRRT2*		unknown	*SIL1*	SIL1	AR
PEX16	PDB8A	AR	*PRX*	CMT4F	AR	*SKOR1*		unknown
PEX19	PDB12A	AR	*PSAP*	PSAP	AR	*SLC12A6*	SLC12A6	AR
PEX2	PDB5A	AR	*PSEN1*	PSEN1	AD	*SLC16A2*	SPG22	XR
PEX26	PDB7A	AR	*PTRH2*		unknown	*SLC17A5*	SLC17A5	AR
PEX3	PDB10A	AR	*PTS*	PTS	AR	*SLC19A3*	SLC19A3	AR
PEX5	PDB2A	AR	*RAB3A*		unknown	*SLC1A3*	EA6	AD
PEX6	PDB4A	AR	*RAB3GAP1*	RAB3GAP1	AR	*SLC25A15*	SLC25A15	AR
PEX7	PDB9B	AR	*RAB3GAP2*	SPG69	AR	*SLC25A2*	BVVLS2	AR
PFN1		unknown	*RAB7*	CMT2B	AD	*SLC25A3*	BVVLS1	AR

Gene	Locus	Mode of Inheritance	Gene	Locus	Mode of Inheritance	Gene	Locus	Mode of Inheritance
PGAP1	SPG67	AR	*RARS2*	PCD8	AR	*SLC25A46*		unknown
PHYH	PHYH	AR	*REEP1*	SPG31/HMN5B	AD	*SLC2A1*		unknown
PIK3R5	PIK3R5	AR	*REEP2*	SPG72	AD/AR	*SLC33A1*	SLC33A1/ SPG42	AR/AD
PLA2G6	NBIA2	AR	*RELN*		unknown	*SLC39A8*		unknown
PLEKHG4	SCA4?	AD	*RNASEH1*		AR	*SLC52A2*	BVVLS2	AR
PLEKHG5	CMTR1C	AR	*RNASEH2B*	RNASEH2B	AR	*SLC52A3*	BVVLS1	AR
PLP1	SPG2/HLD1	XR	*RNASET2*		unknown	*SLC5A2*	RNF216	AR
PLS3	PLS3	unknown	*RNF170*	RNF170	AD	*SLC5A7*	HMN7A	AD
PMM2	CDG1A	AR	*RNF216*	RNF216	AR	*SLC9A1*	SLC9A1	unknown
SMPD1	SMPD1	AR	*TECPR2*	SPG49	AR	*VAPB*	ALS8	AD
SNAP25	SNAP25B	AR	*TFG*	HMSNP	AR	*VARS2*		unknown
SNX14	SNX14	AR	*TGM6*	SCA35	AD	*VCP*	ALS14	AD
SOD1	ALS1	AD	*TH*	TH	AR	*VEGFA*		unknown
SOX10	SOX10	AD	*TMEM138*	JBTS16	AR	*VLDLR*	CAMRQ1	AR
SPAST	SPG4	AD	*TMEM216*	JBTS2	AR	*VPS13A*	VPS13A	AR
SPG11	SPG11	AR	*TMEM231*	JBTS20	AR	*VPS37A*	SPG53	AR
SPG20	SPG20	AR	*TMEM237*	JBTS14	AR	*VPS53*	PCCA2	AR
SPG21	SPG21	AR	*TMEM240*	TMEM240	AD	*VPS54*		unknown
SPG7	SPG7	AR	*TMEM67*	JBTS6	AR	*VRK1*	PCH1A	AR
SPR	SPR	AR	*TOR1AIP1*	TOR1AIP1	AR	*VWA3B*	VWA3B	AR
SPTBN2	SCA5/ SCAR14	AD/AR	*TPP1*	SCAR7	AR	*WDR45*		unknown
SPTBN4	SPTBN4	unknown	*TRAPPC11*		unknown	*WDR48*	SPG60	AR

Gene	Locus	Mode of Inheritance	Gene	Locus	Mode of Inheritance	Gene	Locus	Mode of Inheritance
SPTLC1	HSAN1A	AD	*TRIM2*	CMT2R	AR	*WDR73*		unknown
SPTLC2	HSAN1C	AD	*TRPC3*	TRPC3	unknown	*WDR81*	CAMRQ2	AR
SQSTM1		unknown	*TRPM7*		unknown	*WFS1*	WFS1	AR
SRCAP		unknown	*TRPV4*	CMT2C/SPG36	AD	*WFS1*	WFS1	AD
SRD5A3	CDG1Q	AR	*TCTN3*	JBTS18	AR	*UNC13A*		unknown
SS18L1		unknown	*TDP1*	SCAN1	AR	*UQCRB*	MC3DN3	AR
STUB1	STUB1	AR	*TDP2*		unknown	*UQCRC2*	MC3DN5	AR
STXBP5L	STXBP5L	AR	*TRSP*	TRSP	unknown	*UQCRQ*	MC3DN4	AR
SUFU	SUFU	AR	*TSEN2*	PCH2B	AR	*USP8*	SPG59	AR
SUMF1	SUMF1	AR	*TSEN34*	PCH2C	AR	*VAMP1*	VAMP1	AD
SUN1		unknown	*TSEN54*	PCH2A/PCH4	AR	*WNK1*	HSAN2A	AR
SUN2		unknown	*TSFM*		unknown	*WWOX*	SCAR12?	AR
SURF1	CYTc	AR	*TTBK2*	SCA11	AD	*XPA*	XPA	AR
SVIP	SVIP	AD	*TTC19*	MC3DN2	AR	*XPC*	XPC	AR
SYNE1	SCAR8	AR	*TTC21B*	JBTS11	AR	*XRCC1*		AR
SYT14	SCAR11	AR	*TTPA*	TTPA	AR	*YARS*	CMTDIC	AD
TACO1	CYTc	AR	*TUBA4A*		unknown	*ZFR*	SPG71	AR
TAF15		unknown	*TUBA8*	TUBA8	AD	*ZFYVE26*	SPG15	AR
TARDBP	ALS10	AD	*TUBB2B*		unknown	*ZFYVE27*	SPG33	AD
TBCC		unknown	*TUBB3*	TUBB3	AD	*ZNF423*	JBTS19	AR
TBK1		unknown	*TUBB4A*	DYT4/HLD6	AD	*ZNF592*	SCAR5	AR
TBP	SCA17	AD	*UBQLN2*		unknown	*ZNHIT3*		AR

Gene	Locus	Mode of Inheritance	Gene	Locus	Mode of Inheritance	Gene	Locus	Mode of Inheritance
TCTN1	JBTS13	AR	*UCHL1*	UCHL1	AR			

*genes and loci named as cataloged by OMIM (www.omim.org), AR: autosomal recessive, AD: autosomal dominant, XR: x – linked.

11. Acknowledgements

I am grateful for the participation of HSP patients and family members, without whom our investigations would not have been possible.

First of all, I would like to thank PD Dr. Rebecca Schüle for the great opportunity to work in her lab. Since our initial weekly meetings, I have been able to steadily expand my skills through her continuous support and superior expertise.

I would also like to thank all the members of the Schüle lab for the immense support and nice working atmosphere in the “Denkzelle”.
Especially Jennifer Reichbauer, who taught me most of the techniques in my first months in her caring and patient manner.
Thank you, Selina Reich, for introducing me into Western Blotting, for all the time you invested in my project and for answering all my questions. To me you are a true inspiration for good scientific practice in research.
Melanie, thank you very much for being my best working buddy in the finishing experiments and thank you for almost making all the working weekends we spent in the lab something to look forward to.
A very special thank you to Maike Nagel as the best colleague, motivator and supervisor one could ever have. You are an absolute role model for me. Without you this work would never have been finished and I am very grateful that we call each other friends.

Additionally I would like to thank the whole AG “Schüle/Synofzik/Schöls” group for all the nice talks and funny moments we shared at numerous lunch breaks or after work events together.

Last but not least special thanks goes to my family and friends for their unconditional support and believe in me.